JBC Papers in Press. Published on May 31, 2018 as Manuscript RA118.002038
The latest version is at http://www.jbc.org/cgi/doi/10.1074/jbc.RA118.002038

Epigallocatechin-3-gallate remodels apolipoprotein A-I amyloid fibrils into soluble oligomers in the presence of heparin

David Townsend[a], Eleri Hughes[a], Geoffrey Akien[a], Katie L. Stewart[b,c], Sheena E. Radford[b,] David Rochester[a] and David A. Middleton[a]*

[a]Department of Chemistry, Lancaster University, Lancaster, LA1 4YB, United Kingdom [b]Astbury Centre for Structural Molecular Biology, School of Molecular and Cellular Biology, Faculty of Biological Sciences, University of Leeds, Leeds LS2 9JT, United Kingdom.

[c]Present address: Department of Physics, Emory University, Atlanta GA 30322.

Running title: *Remodeling of apoA-I amyloid by heparin and EGCG*

*To whom correspondence should be addressed: David A. Middleton: Department of Chemistry, Lancaster University, Lancaster, LA1 4YB, United Kingdom: d.middleton@lancaster.ac.uk
Tel: +44 1524 594328

Key words: atherosclerosis; apolipoprotein; solid-state NMR; circular dichroism; transmission electron microscopy; polyphenol; glycosaminoglycan; amyloid fibrils.

Abstract

Amyloid deposits of wild-type apolipoprotein A-I (apoA-I), the main protein component of high-density lipoprotein, accumulate in atherosclerotic plaques where they may contribute to coronary artery disease by increasing plaque burden and instability. Using CD analysis, solid-state NMR spectroscopy, and transmission EM, we report here a surprising cooperative effect of heparin and the green tea polyphenol (–)- epigallocatechin-3-gallate (EGCG), a known inhibitor and modulator of amyloid formation, on apoA-I fibrils. We found that heparin, a proxy for glycosaminoglycan (GAG) polysaccharides that co-localize ubiquitously with amyloid *in vivo*, accelerates the rate of apoA-I formation from monomeric protein and associates with insoluble fibrils. Mature, insoluble apoA-I fibrils bound EGCG (K_D = 30 ± 3 μM; B_{max} = 40 ± 3 μM), but EGCG did not alter the kinetics of apoA-I amyloid assembly from monomer in the presence or absence of heparin. EGCG selectively increased the mobility of specific backbone and side-chain sites of apoA-I fibrils formed in the absence of heparin, but the fibrils largely retained their original morphology and remained insoluble. By contrast, fibrils formed in the presence of heparin were mobilized extensively by the addition of equimolar EGCG, and the fibrils were remodeled into soluble 20-nm-diameter oligomers with a largely α-helical structure that were nontoxic to human umbilical artery endothelial cells. These results argue for a protective effect of EGCG on apoA-I amyloid associated with atherosclerosis and suggest that EGCG-induced remodeling of amyloid may be tightly regulated by GAGs and other amyloid co-factors *in vivo*, depending on EGCG bioavailability.

Introduction

Amyloidosis is a group of disorders characterized pathologically by the extracellular accumulation of insoluble protein fibrils with a cross-β structural motif. Systemic amyloidosis affects several organs and tissues, whereas localized amyloid is confined to a single organ. In each case the clinical manifestations depend on the precursor protein (1). Localized amyloid deposits of the Aβ peptide in Alzheimer's brains have been characterized extensively, although the relationship between misfolded Aβ and disease remains unresolved. The pathological consequences of systemic amyloidosis are less ambiguous and often involve irreparable damage to major organs at the end-stage of disease. Systemic amyloid derived from apolipoprotein A-I (apoA-I), the major protein component of the high density lipoprotein (HDL) complex

which transports cholesterol to the liver, was identified in the 1990's as a hereditary condition related to several mutant forms of the protein which are susceptible to protease digestion, misfolding and aggregation (2,3). More recent evidence has shown that fibrils of wild-type apoA-I also accumulate spontaneously in the plaques of atherosclerosis and may contribute to the condition (4-7). Lipid-deprived apoA-I can undergo an alternative folding pathway in which the protein self-assembles into amyloid (8,9), resulting in loss of its atheroprotective properties and the accumulation of potentially damaging amyloid plaques in vital organs and vasculature. The high incidence of fibrillar apoA-I associated with atherosclerotic lesions suggests that amyloid deposition may decrease plaque stability and contribute to the progression of atherosclerosis (6,7,10,11).

Native, functional apoA-I has a predominantly α-helical structure, but the fibrillar aggregates exhibit a combination of α-helical and β-sheet conformations as revealed by circular dichroism and solid-state NMR spectroscopy (12). ApoA-I aggregation *in vitro* is accelerated under acidic conditions (11) and by myeloperoxidase-catalysed oxidation (13) associated with inflammatory diseases such as atherosclerosis. Whether the enhanced aggregation kinetics at low pH is pathologically significant is not clear, although a small but significant pH reduction (to 7.15) has been observed *ex vivo* in calcified areas of lesions (14). In addition, heparin, a member of the glycosaminoglycan (GAG) polysaccharides that co-localize ubiquitously with amyloid *in vivo* (15,16), accelerates the formation of ordered apoA-I fibrils in a concentration-dependent manner (11,12). Generally, heparin is known to increase the rate of amyloid fibril formation (17,18), stabilize fibrils (19,20) and reduce amyloid toxicity (21,22). The GAG chains of proteoglycans in the arterial intima associate with apoA-I in the advanced stages of atherosclerosis (23) and the accumulation of high local apoA-I concentrations may contribute to the formation and retention of amyloid deposits. The native structure of apoA-I is stable for at least 24 h above pH 7 (12), but at pH 4-5 in the presence of heparin aggregation is virtually instantaneous.

Polyphenols from green tea, including (–)-epigallocatechin-3-gallate (EGCG), are flavonoids that are considered to have beneficial protective effects on cardiovascular health and against atherosclerosis, resulting from their anti-oxidant and anti-inflammatory properties (24,25). EGCG has also been shown to modulate the aggregation kinetics of several amyloidogenic proteins, including Aβ, α-synuclein and amylin, and directs the assembly pathway toward the formation of large, off-pathway and non-toxic oligomers (26-28). EGCG remodels insoluble amyloid fibrils into amorphous aggregates with reduced toxicity to mammalian cells (29). Oxidized and unoxidized EGCG molecules bind to amyloid fibrils through engagement of hydrophobic sites (30) and polar contacts (31,32), but autooxidation of EGCG appears to invoke covalent cross-linking with the fibrils that stabilize the remodelled aggregates (33). These properties of EGCG offer potential therapeutic benefits, and clinical trials of EGCG for the treatment of early-stage Alzheimer's and antibody light chain (AL) amyloidosis have been completed or are currently active. Low bioavailability and intestinal and hepatic metabolism are considered potential difficulties of medical utilization of the unmodified natural product (34,35). Recently it was shown that EGCG disaggregated fibrils of the G26R (Iowa) mutant of apoA-I and also inhibited fibril growth, as assessed by the amyloid-reactive dye thioflavin T (ThT) (36). The effects were also replicated on the N-terminal 1-83 peptide fragment of both the Iowa mutant and wild-type protein. A detailed molecular analysis of EGCG with wild-type apoA-I associated with atherosclerosis, however, has not been reported.

Here, we show that EGCG interacts with fibrils of wild-type, full-length apoA-I preferentially over other green tea components without modulating apoA-I fibril growth kinetics. Circular dichroism (CD), solid-state NMR spectroscopy (ssNMR) and transmission electron microscopy (TEM) reveal that EGCG remodels apoA-I fibrils into soluble non-toxic oligomers when fibrils are formed in the presence of heparin, but not when fibrils are formed in the absence of heparin. This surprising synergistic effect of EGCG and heparin may offer a means of influencing the deposition of apoA-I amyloid associated with atherosclerosis and possibly other amyloid known to associated with GAGs *in vivo*.

Results

Heparin associates with apoA-I fibrils: Wild-type apoA-I is known to undergo ThT-responsive aggregation in solution at pH 4 that is accelerated by the addition of heparin (11,12). Transmission electron microscopy (TEM) indicates that incubation of apoA-I alone at pH 4 for 3 days results in the deposition of fibrils (Figure 1A, left) and distinct deposits of more amorphous material (Figure 1A, right), whereas incubation of apoA-I with a 2-fold molar excess of heparin (assuming a mean M_r of 14.5 kDa) results in only fibrils. The fibrils in the absence of heparin are 7-15 nm in diameter and fibrils in the presence of heparin are distributed from 10-21 nm in diameter, although the mean widths are not significantly different (Figure 1C). Heparin may therefore either influence the aggregation process and/or may co-localize with the fibrils, as found for other amyloid-forming proteins (37-41). None of the TEM images showed any evidence of nanoscale structures other than fibrils or amorphous aggregates, even after shorter incubation times.

Evidence for heparin binding to the fibrils was obtained using a heparinase I assay (42), in which the concentration of heparin remaining in solution was determined after incubation with monomeric apoA-I and removal of the fibrils formed after 3 days by sedimentation. From an initial concentration of 1 mg/mL, heparin is progressively removed from solution by increasing amounts of protein (Figure 1D). Furthermore, apoA-I fibrils formed in the presence of heparin doped with a heparin-fluorescein conjugate showed strong fluorescence enhancement over the background protein fluorescence (Figure 1E), consistent with co-localization of the fluorophore and fibrils. The results thus show that heparin binds to apoA-I during or after its aggregation into amyloid and precipitates concomitantly with the insoluble fibrils.

Selective binding of green tea polyphenols to apoA-I fibrils: To investigate whether apoA-I fibrils bind EGCG and other polyphenols from green tea, an aqueous green tea solution was prepared by microwave extraction of the dried leaves. A HPLC method was developed to quantify green tea polyphenol and caffeine binding to pre-formed fibrils. Insoluble fibrils prepared in the absence of heparin at pH 4 (1 mg/mL monomeric apoA-I) were suspended in an aqueous solution of green tea (1 mL) and incubated for 12 h with gentle agitation before centrifugation and retention of the supernatant for analysis. Control samples of the tea extract solution alone were treated in the same way. Reverse-phase HPLC of the control solution resolves several major components which were identified by mass spectrometry (12) and quantified with reference to a standard mixture of eight green tea catechins of known concentration (Figure 2 and Table 1). Comparison of the peaks for the fibril-treated and control solutions reveals that specific components are removed from solution by binding to the fibrils. The major component, EGCG (peak 5), reduces to <50 % of its initial concentration after sedimentation of the apoA-I fibrils (Figure 2B) and epicatechin-3-gallate (ECG) (peak 7) also shows appreciable binding. The 3-gallate moiety, therefore, appears to enhance the affinity of the polyphenols to associate with apoA-I fibrils. EGCG and ECG are also removed from the green tea extract when incubated with fibrils of the 40-amino acid amyloid-β peptide (Aβ40) (Figure 2C), confirming the affinity of these polyphenols for amyloid fibrils derived from different proteins. Titration of apoA-I fibrils (36 μM monomer equivalent concentration) with a solution of pure EGCG yields an apparent dissociation constant (K_d) and saturation binding concentration (B_{max}) of 40 ± 4 μM and 45 ± 5 μM, respectively (Figure 2D). Similar values (K_d = 30 ± 3 μM; B_{max} = 35 ± 3 μM) were obtained when EGCG was added to the monomeric protein and incubated for 48 h before removing the insoluble protein by centrifugation. In both cases the saturation binding concentration of EGCG is approximately equimolar.

EGCG does not alter the aggregation kinetics of apoA-I: We next used ThT fluorescence to determine whether EGCG influences the kinetics of aggregation of apoA-I under conditions previously reported to favor apoA-I assembly into amyloid (11,12). At pH 4, incubation of apoA-I alone results in a slow enhancement of ThT fluorescence (Figure 2E). The addition of heparin, however, results in a rapid enhancement of ThT fluorescence, followed by a further, more gradual increase (Figure 2E) (in the absence of protein heparin does not affect ThT fluorescence

(data not shown)). Previous work has shown that the rapid fluorescence enhancement induced by heparin reflects an increase in insoluble, partially fibrillar protein (12). A repeat of the measurements in the presence of EGCG (2-fold molar excess over the protein) or green tea extract (containing an estimated 2-fold molar excess of EGCG with respect to the protein concentration) showed that EGCG and the leaf extract do not affect the aggregation kinetics of apoA-I, regardless of whether heparin is present. This observation contrasts with the reported inhibitory effect of EGCG on a peptide fragment of the $apoA_{Iowa}$ variant (36) and on the amyloid-β peptide (29,43). Equimolar EGCG is sufficient to cause a marked reduction in ThT fluorescence in the presence of MAβ40 (the 40-residue amyloid-β peptide with an additional N-terminal methionine) without affecting the lag time or elongation rate (Figure 2F), consistent with the known ability of EGCG and ThT to compete for the same binding site (33).

Enhancement of backbone and side-chain dynamics within fibrillar apoA-I: A more detailed analysis was next carried out to determine whether EGCG modulates the structure of the apoA-I fibrils as it does for other fibrillar proteins (28,29,33,44). Solid-state NMR (SSNMR) has recently revealed interesting structural features of apoA-I fibrils in which the duplication of some cross-peaks in 2D ^{13}C-^{13}C spectra suggest that the fibrils comprise a mixture of α-helical elements and new, amyloid-like β-sheet elements within the fibril architecture (12). 2D ^{13}C-^{13}C magic angle spinning (MAS) ssNMR spectra of ^{13}C-labeled apoA-I fibrils (Figure 3A), prepared at pH 4 alone or in the presence of heparin, or at pH 6 after protein oxidation by hydrogen peroxide, exhibit similar features, including the same duplication of peaks for specific amino acids, including alanine, threonine, leucine and valine. The duplicated peaks occur in approximately the same intensity ratios for each sample, as shown by the slices through the Cα-Cβ cross-peaks for alanine (Figure 3B), suggesting that the α-helical and β-sheet elements, which give rise to the differences in chemical shift observed (12), occur within a single, common fibril architecture (see Discussion).

After adding EGCG to apoA-I fibrils formed at pH 4 in the absence of heparin, several cross-peaks disappear from the ^{13}C-^{13}C spectrum, specifically the cross-peaks assigned to valine, threonine and alanine in α-helical environments and the proline Cγ-Cδ cross-peak (Figure 4A, left, red spectrum). The remaining cross-peaks occur at the same positions as in the spectrum of untreated apoA-I fibrils (Figure 4A, left, black spectrum). The changes in the spectrum can be interpreted as a selective structural remodelling of the fibrils, caused by exposure to EGCG. The same cross-peaks disappear from the spectrum of apoA-I fibrils assembled in the presence of EGCG (Figure 4A, right), indicating that similar fibril remodelling occurs regardless of whether EGCG is present at the onset or added at the end-point of aggregation.

An explanation for these observations is that EGCG increases protein mobility over selective regions within the fibrils: this is because cross-peaks in the ^{13}C-^{13}C spectrum arise from dipolar coupling between ^{13}C nuclei and if the couplings are reduced by increased motional fluctuations then the cross-peaks can weaken in intensity or disappear. Increased mobility was tested using ^{1}H-^{13}C INEPT ssNMR, which detects signals only from dynamic regions of fibrillar proteins (45). A 1D INEPT spectrum of EGCG-treated fibrils reveals several sharp peaks attributable to the mobile regions of the protein (Figure 4B, red), but the 1D INEPT spectrum of fibrils in the absence of EGCG fails to detect any signals after 24 h of measurement (Figure 4B, black). These results indicate protein mobility within the untreated fibrils is enhanced after exposure to EGCG. A 2D extension of the ^{1}H-^{13}C INEPT experiment on the EGCG-treated fibrils enables some of the peaks to be assigned to specific amino acids (Figure 4C). Most of the resonances occur in the amino acid side-chain region of the spectrum (principally from methyl-bearing or polar/charged side chains) and there is much less signal intensity in the Cα/Hα region, which implies that most of the protein backbone remains relatively constrained. The resolved $^{13}C\beta$ chemical shifts of the mobile leucine, threonine, asparagine, alanine and serine side chains are consistent with these residues occupying an α-helical structure (Figure 4C and Table 2).

We next obtained a 2D ^{1}H-^{13}C INEPT spectrum of EGCG-treated apoA-I fibrils formed in the presence of heparin (Figure 4D, blue). Surprisingly, many more signals are observed than are seen in the spectrum of EGCG-treated

fibrils formed in the absence of heparin (Figure 4D, red), particularly in the backbone Hα/Cα region shown in Figure 4D. This observation is consistent with even greater mobilization of the fibrils formed when heparin is present, including enhanced dynamics of the protein backbone residues. Heparin and EGCG therefore appear to have an unexpected synergistic effect on increasing apoA-I mobility within protein fibrils. A simulated INEPT spectrum (Cα-Hα region only) based on all 243 apoA-I residues in an α-helical environment (Figure 4E) implies that one would expect many more resonances to be observed if the protein was fully mobilized to an equal extent across the entire sequence.

EGCG remodels heparin-promoted apoA-I fibrils into oligomers: We next examined whether the increased mobility of apoA-I aggregates could originate from resolubilization of the fibrils by EGCG. CD spectroscopy was used to detect any structured soluble protein that may be released from the fibrils after binding EGCG. Fresh samples of fibrils formed (at pH 4) after 3 days were incubated with equimolar EGCG for 12 h and the remaining insoluble material was removed by centrifugation before analysis of the supernatant by CD. For control experiments the EGCG solution was replaced with McIlvaine buffer alone. Little signal is observed in the far UV CD spectra of the control samples or in the spectra of EGCG-treated fibrils formed in the absence of heparin to which EGCG had been added (Figure 5A) and reliable analysis of the secondary structure could not be performed. Hence the concentration of soluble protein is low in these samples and most of the protein was removed in the insoluble fraction. In marked contrast, when fibrils formed in the presence of heparin are treated with EGCG, the supernatant produces a strong signal in the far UV CD that is characteristic of structured, soluble protein with α-helical content (Figure 5A, red solid line). Quantitative analysis of the spectrum using the CONTINILL fitting algorithm (Figure 5B, red lines) indicates that the structure of the soluble material is ~75 % α-helical. The CD spectrum of the native protein (Figure 5B, black lines), which is stable in solution at pH 7 (12), indicates a similar helical content of 68 %. Hence EGCG results in the shedding of molecules with a predominantly α-helical structure from fibrils formed with heparin, but it is not clear whether the mobilized protein reverts to its native structural state. Dynamic light scattering (DLS) analysis of the EGCG-treated apoA-I fibrils revealed species with a hydrodynamic radius distribution of 5-25 nm results from dissociation of fibrils assembled with heparin whereas none of the other buffer or EGCG-treated samples released soluble species of this size (Figure 5D). No species larger than 25 nm were released from the fibrils. Together, the SSNMR, CD and DLS data indicate that EGCG remodels insoluble apoA-I fibrils into soluble α-helical species much more readily when the fibrils have formed in the presence of heparin.

The EGCG-treated fibrils (formed alone or with heparin) were next centrifuged and the morphologies of the soluble species in the supernatant and the insoluble material in the pellet were visualised using negative stain TEM. For the fibrils formed alone, exposure to EGCG does not disrupt the fibrillar morphology within the insoluble fraction and the soluble fraction is virtually free of visible protein aggregates in the 5-25 nm range (Figure 6A). By contrast, fibrils formed in the presence of heparin are remodelled by EGCG into small, granular structures which remain insoluble, whilst a proliferation of soluble spherical oligomer-like species, 20-30 nm in diameter are now also present (Figure 6B). No such species of apoA-I were observed at any point in the absence of EGCG. Indeed, apoA-I assembly into fibrils is instantaneous in the presence of heparin at pH 4 and is unlikely to proceed via oligomeric intermediates. The combined effect of heparin and EGCG appears to extensively remodel the apoA-I aggregates into unique α-helical oligomers that are otherwise not observed in the aggregation pathway. In the absence of heparin the effect of EGCG is less pronounced and more selective for specific regions of the protein. For comparison, we also visualised the effect of EGCG on Aβ40 fibrils (formed by seeding their growth in the absence of heparin). The results showed that fibrils are fragmented into smaller, spear-like structures after treatment with EGCG, as reported previously (29), although the smaller oligomeric and amorphous species observed in the same work are not observed here (Figure 6C).

We next investigated whether the soluble apoA-I aggregates released by EGCG are toxic to cells at varying molar ratios of EGCG to protein. A cell viability assay using the cellular

dehydrogenase-sensitive dye WST-8 was used to assess the cytotoxicity of EGCG-treated apoA-I fibrils to human umbilical artery endothelial cells (Figure 7, A and B). Insoluble fibrils (7.2 μM monomer equivalent), formed in the absence or presence of 14.4 μM heparin, were treated with EGCG up to a 5-fold molar excess (i.e., 36 μM) of the polyphenol over the protein, and the solutions were added to the cells after removal of the extant insoluble material. Cell viability is not impaired when apoA-1 fibrils are exposed to equimolar or lower concentrations of EGCG and this is apparent whether or not ApoA-I fibrils are formed alone or with heparin (Figure 7, A and B). Fibrils treated with higher concentrations of EGCG (2-5 fold excess) do show some impairment of cell viability (Figure 7, A and B). However, control measurements on cells treated with 36 μM EGCG, 14.2 μM heparin or 36 μM EGCG and 14.2 μM heparin together, all in the absence of apoA-I, indicate that the cytotoxic effect at higher EGCG concentrations is a direct result of excess polyphenol and is not related to the presence of apoA-I (Figure 7C). SSNMR, DLS, CD and TEM all agree that apoA-I fibrils formed in the presence of heparin release soluble oligomers after treatment with equimolar EGCG. Here the data indicate clearly that the soluble oligomers are not cytotoxic.

EGCG interacts with monomeric apoA-I but not with heparin: Exposure of apoA-I fibrils formed in the presence of heparin releases heparin into the aqueous phase in an EGCG concentration-dependent manner (Figure 7D). We therefore investigated whether EGCG interacts with heparin as well as with the monomeric protein. A solution-state waterLOGSY NMR experiment was used to detect EGCG binding to heparin and, separately, to monomeric apoA-I. In the waterLOGSY experiments bulk water magnetization is transferred to EGCG if it binds to the larger protein or polysaccharide molecule, resulting in resonances for EGCG that are of opposite sign to non-interacting compounds. We here used the internal reference trimethylsilylpropanoate (TSP) as the non-binding molecule, comparing the sign of the peak at 0 ppm with EGCG aromatic resonances. WaterLOGSY spectra of EGCG alone and in the presence of heparin or apoA-I were compared with the corresponding 1D ^{1}H spectra (Figure 8). As expected, peaks from TSP and EGCG are narrow and have the same sign in the 1D and waterLOGSY spectra in the absence of either of the macromolecules (Figure 8A). In the presence of apoA-I the peaks from EGCG broaden and take the opposite sign to the TSP peak in the waterLOGSY spectrum (Figure 8B), consistent with EGCG-protein binding, whereas the spectra of EGCG in the presence of heparin do not indicate an interaction between the two molecules (Figure 8C).

Finally we investigated whether EGCG interacts with apoA-I as the unoxidized polyphenol or in the form of oxidized quinones. The reactive form of EGCG influences whether the interaction with apoA-I is covalent or non-covalent. EGCG is able to undergo auto-oxidation, generating quinones and superoxide, which in turn promotes further EGCG oxidation (46). The quinones can self-react to form polymeric species via intermolecular cross-linking, and can also react covalently with available SH or NH_2 groups of proteins (47). Under oxygenated conditions in solution at pH 7.4, EGCG was shown to be fully oxidized after a 6 h incubation period (33). Here we assessed whether the low pH conditions used in the aggregation and re-solubilization studies protected against EGCG oxidation. EGCG polyphenol absorbs maximally at ~275 nm, but oxidation above pH 7 results in a color change and shift in the absorbance maximum to 320 nm (48). Here, at pH 4 the maximum absorbance of EGCG alone in solution (72 μM) remained unchanged for 3 days with no evidence of additional absorbance bands appearing above 320 nm (data not shown), indicating that the polyphenol alone remains stable under these conditions. We next used LCMS to determine whether EGCG undergoes oxidation over time in the presence of apoA-I. The LCMS chromatograms for fresh and aged (up to 3 days) solutions of EGCG and apoA-I, with or without heparin showed an intense peak at 7.65 min (Figure 9A). The peak area does not decrease significantly when measured after incubation of EGCG and apoA-I for 1, 2 and 3 days (in fact, a slight unexplained increase is observed) and no additional peaks consistent with oxidation or degradation products can be seen (Figure 9B). The [M+H]+ and [M-H]- peaks in the positive and negative polarity scans respectively were used to obtain extracted ion chromatograms (XIC) from which peak integration values were

obtained. For both positive and negative ionisation modes the base peak observed at 7.65 min was assigned to a commonly observed adduction of unmodified EGCG at 459.0903 m/z and 457.08 m/z, respectively (Figure 9C). Finally we checked whether fibrils of apoA-I could be covalently modified by EGCG, using ssNMR and ^{15}N-labelled protein (in the absence of heparin). The ^{15}N MAS NMR spectrum of apoA-I fibrils alone exhibit clear peaks from the lysine and arginine NH_2 groups (Figure 9D), which remain unchanged when the fibrils were incubated with EGCG for 1 day. A decrease in the lysine peak intensities and the appearance of peaks at higher chemical shifts (>120 ppm for Schiff bases) would be expected if the primary amines were covalently modified. We conclude, therefore, that EGCG does not oxidize or covalently modify apoA-I under the conditions applied here.

Discussion

In the above experiments we set out to investigate whether EGCG exerts a potentially protective effect on apoA-I amyloid that is associated with atherosclerosis, as reported for several other amyloidogenic proteins associated with disease (49,50). Studies on Aβ40/42, α-synuclein, amylin, huntingtin and transthyretin have all shown a common ability of EGCG to bind to the oligomeric and multimeric forms of amyloid, to inhibit fibril assembly and to prevent formation of toxic structures (28,29,51-55). In the case of both Aβ40/42 and α-synuclein, EGCG prevents fibrillogenesis by binding preferentially to unfolded protein, directing assembly towards off-pathway non-toxic oligomers and thereby preventing formation of toxic oligomers and protofibrils (29). When added to pre-formed aggregates, EGCG can also alter their β-sheet conformation and convert aggregates into small, non-toxic amorphous aggregates (28,29). Remodelling of amyloid from several different proteins may also involve auto-oxidation of EGCG, which can result in covalent modification of free amine groups, although this mechanism is not the major driving force for the structural remodelling (33). Here we have identified similarities but also reveal a remarkable and hitherto unknown synergy between the effect of this polyphenol and the GAG heparin on the behaviour of an amyloid aggregate.

In order to rationalize our observations it is convenient to consider the structural features of apoA-I aggregates at the molecular level. ApoA-I forms ThT-responsive aggregates under oxidative or acidic conditions and the process is accelerated by the GAG analogue heparin, which co-localizes with the fibrils (Figure 1). In the latter regard, apoA-I behaves similarly to Aβ, α-synuclein and amylin, all of which assemble into amyloid more rapidly in the presence of heparin (42,56-59). In some cases heparin decorates the surface of the fibrils, such as in salmon calcitonin fibrils (60) and in the 3Q fibrils of Aβ40 (42,45,59), whilst in other cases heparin does not form a stable complex with the insoluble fibrils (61). The apoA-I aggregates formed under the conditions employed here are predominantly fibrillar (~10 nm diameter) which form alongside amorphous material that is known to form around the native protein's pI of 5.2 (62). The rate of fibril formation is rapid at pH 4, which is a much more acidic pH than that measured in *ex vivo* lesions (14). However, the fibrillar end-point appears to be structurally identical to fibrils formed at a higher, more physiological pH after myeloperoxidase-catalysed oxidation or after incubation of unmodified protein for longer periods (12). The low pH conditions applied here are for the purpose of expediting the fibrillar end-point rather than for replicating the lesional microenvironment. SSNMR spectra reveal the co-existence of α-helical and β-sheet secondary structural elements in approximately the same proportions in the apoA-I aggregates, regardless of the aggregation conditions employed (Figure 4). We believe that both structural elements occur within a single fibrillar architecture, such that each protein molecule within an aggregate possesses both β-sheet and α-helical regions. An alternative explanation, that apoA-I assembles via two divergent pathways into discrete assemblies of extensively β-sheet protein and predominantly α-helical protein, is also possible.

EGCG is the major polyphenol component of green tea known bind to pre-formed aggregates of apoA-I. EGCG has been shown to interact with Ile, Phe and Tyr residues, preventing the hydrophobic contacts required for conversion to a stable β-sheet conformation and enabling disaggregation of pre-formed amyloid fibrils (63). Aβ40 assembles into fibrils via

conformationally labile states, potentially enabling access of EGCG to block hydrophobic contacts, but the compact native structure of lipid-free apoA-I (64) and its ability to form abundance of hydrophobic contacts stabilizing the native helical bundle may overcome any inhibitory effect that EGCG may exert.

The most striking outcome of this work is the effect of heparin on the ability of EGCG to restructure aggregates of apoA-I. In the absence of heparin, EGCG selectively mobilizes alanine, valine and threonine sidechain within α-helical regions and proline residues are also affected (Figure 4). Proline residues occur throughout the apoA-I sequence and punctuate the helical regions with hinges, enabling the protein to form the annular belt-like structure associated with HDL (65). The INEPT ssNMR experiments indicate that the amino acid side-chains are mobilized to a greater extent than the backbone (Figure 4C), which implies that EGCG acts largely peripherally, leaving the stable β-sheet core of the fibrils intact. When EGCG is added to fibrils assembled in the presence of heparin its remodelling effect is amplified significantly, yielding an abundance of spherical oligomers ~ 20 nm in diameter that are non-toxic to human endothelial cells.

How do heparin and EGCG cooperate to remodel apoA-I fibrils? A direct interaction between EGCG and heparin was ruled out by waterLOGSY NMR experiments. Heparin was also shown to enhance the aggregation kinetics of apoA-I (Figure 2D), likely by the high local ionic strength micro-environment of heparin combined with the directionality and periodicity of its anionic groups that may act as a template for apoA-I assembly (66). The SSNMR spectra do not support major structural differences in the fibrils formed with or without heparin (Figure 3), but it is possible that subtle structural modifications by heparin could open up additional binding sites for EGCG. Alternatively, the partial mobilization of the fibrils by EGCG seen in the absence of heparin could be amplified by heparin when bound to the fibril surface.

The lack of cellular toxicity of the soluble oligomers promoted by EGCG in the presence of heparin, when taken together with their absence during the fibril assembly pathway, suggests that these are unique species formed specifically by the action of EGCG on the fibrils, rather than a regeneration of on-pathway, toxic annular oligomers that are observed for other amyloidogenic peptides and proteins (67). Annular species have been observed when methionine-oxidized apoA-I undergoes aggregation at pH 6 (68), but these are not formed reproducibly and are in much smaller amounts than the profusion of oligomers observed here. Why the oligomers are not toxic is unclear. EGCG binds to pre-formed oligomers of α-synuclein and protects against their inherent cytotoxicity by inhibiting oligomer-membrane interactions (69). A similar mechanism might underlie the observations on apoA-I, but cannot easily be tested owing to the inability to prepare pre-formed oligomers in the absence of EGCG.

The ability of EGCG to reproduce the observed effects *in vivo* is dependent on the available concentration of EGCG in blood and in the aortic intima. EGCG reaches maximum plasma concentration 2 h after drinking a cup of green tea, but the steady-state concentration may be much higher for frequent green tea drinkers (70). Studies with human serum albumin (HSA) indicate that EGCG binds to two high affinity sites (K_D = 22 μM) and several additional low-affinity surface sites (mM K_D), suggesting that plasma concentrations of HSA (~600 μM) can bind up to 98 % of EGCG (71). This would account for the slow metabolism of EGCG, but could also restrict its availability for interactions with amyloid proteins, including Aβ, α-synuclein and apoA-I. However, as Eaton and Williamson point out in their recent work (71), the weaker (millimolar) binding implies fast off-rates and the weakly bound EGCG would dissociate at a rate of 100 s^{-1} or faster (assuming the association rate is at the diffusion-limit). Hence the exchange of EGCG between HSA and tissue is likely to be rapid. With regard to the atherosclerotic environment, HSA and its cargo can enter the proteoglycan-rich intimal layer of the aorta from the luminal and adventitial sides (72), and the concentration of HSA in the interstitial space is approximately half that in plasma (73). Further detailed experiments, beyond the scope of this work, will be required to establish whether the local acidic environment of atheromatous tissue enhances the release of sufficient EGCG from HSA for interaction with fibrillar apoA-I. It is interesting to note, however, that EGCG affinity for bovine serum albumin decreases in acidic solution (74).

In summary, we demonstrate here an unusual interplay between apoA-I, EGCG and heparin that, together, mobilize fibrils and result in the shedding of non-toxic oligomers that does not occur in the presence of either ligand alone. The results add a layer of complexity in considering the effects of small molecules on the progress of amyloid assembly and amyloid-associated cytotoxicity in a cellular context, wherein other components such as GAGs may affect the outcome of administration of a small molecule. Indeed number of natural GAG variants have been identified as co-localizing with amyloid plaques, including chondroitin sulfate (75-77), dermatan sulfate (78), and keratan sulfate (79), all of which, like heparin and HS, contain poly-sulfated disaccharide units. Whether fibril mobilization is a benefit or a threat may also be reconsidered, where reduction of fibril load may be of greater benefit than the production of small amounts of oligomers, which may be degraded, further dissociated by binding to molecular chaperones *in vivo.* Whichever the outcome, the results presented suggest that it may now be appropriate to re-evaluate the wider, potentially protective effects of EGCG as an amyloid remodelling agent, by considering the synergistic effects of GAGs and other ubiquitous co-factors of amyloid *in vivo*.

Methods and Materials

Protein expression and fibril formation: Expression of N-terminally His-tagged apoA-I was carried out by following previously published methods (80,81). A pNFXex expression vector coding for human apoA-I with an N-terminal His tag (kindly provided by Dr M. Oda, Oakland Research Institute, USA) was transformed into *E. coli* BL21 (DE3) cells (Agilent Technologies) and grown at 37°C in LB media containing 100 μg/ml ampicillin (Melford Laboratories). The plasmid construct expresses apoA-I with an E2D mutation enabling removal of the His-tag by cleavage of the acid-labile Asp2-Pro3 peptide bond with formic acid, leaving the native residues 3-243. The remaining expression and purification methods are described in ref (12).

ApoA-I fibrils were formed from up to 36 μM apoA-I incubated in McIlvaine Buffer (165 mM Na_2HPO_4, 17.6 mM citrate, pH 4), typically for 3 d (unless specified otherwise), alone or in the presence of a 2-fold molar excess of heparin (IdoA(2S)-GlcNS(6S) 14-15 kDa, >70 %, Iduron). Expression of MAβ40 and fibril formation by seeding with the 3-fold symmetrical (3Q) morphology was carried out as described previously (45).

Isolation of polyphenol compounds from green tea: Green tea (2 g, Twining's™ pure) was added to 40 mL of water. The solution was microwaved at 900 W of power for 2 cycles of 30 seconds, followed by 4 cycles of 15 seconds with a minute between each heating. The solution was filtered through a 1μm filter paper (Whatman) and filtered with a 20 μm corning syringe filter. The solution was then freeze-dried until further use.

HPLC analysis of green tea compounds: A stock solution of the green tea extract was prepared by dissolving the lyophilized material in water (7.2 mg/ml) for analysis by reverse-phase high performance liquid chromatography (HPLC). The pH of the solution was 7.5. A standard mixture of 8 green tea catechins (each at 100 μg/mL) (Sigma, UK) was used as a reference set to assist in the assignment of HPLC peaks. Separation was performed on a NexeraX2 UHPLC (Shimadzu) system with a mobile phase of 0.1 % orthophosphate in ultrapure water (A) or in acetonitrile (B), whilst the static phase consisted of a Shim-pack XR-ODS 2.2 μm, 3.0 x 50 mm) reverse phase column. The green tea stock solution was injected after a further 10-fold dilution in water and the standard catechin solution was injected without further treatment. The injection volume was 10 μL in both cases. The gradient elution, at a flow rate of 1 mL/min consisted of 0-3 minutes (5% of B), 3-10 min (5-20 % B), 10-13 min (20-50 %) and 13-13.1 min (50-5 % B) and 13.1-20 min (5 % B). Absorbance intensity was measured at 275 nm with a band width of 4 nm.

For determination of green tea polyphenol binding to apoA-I, a 200 μL suspension of apoA-I fibrils (36 μM monomer equivalent) was centrifuged for 10 min at 12,000 *g*. The green tea stock solution was diluted 200-fold in water and 200 μL was added to the fibrillar pellets followed by incubation with agitation at 37°C for 24 h. The fibrils were pelleted through centrifugation and the supernatant removed without further treatment for analysis by HPLC

as described above.

LCMS Analysis of EGCG: ApoA-1 (36 μM) plus 72 μM EGCG was acidified at pH 4 in the presence and absence of 72 μM heparin and fibrils allowed to form over 3 days at 37 °C with shaking. At intervals of 0, 1, 2 and 3 days, the samples were centrifuged and 50 μl aliquots of supernatant taken for further testing by LCMS. Mass spectra were acquired using a Shimadzu LCMS-IT-TOF mass spectrometer. LC separations were performed using a Shimadzu NexeraX2 UHPLC instrument consisting of a DGU-20A5R degassing unit, two LC-30AD liquid chromatography pumps, a SIL-30AC autosampler, and a CTO-20AC column oven. Separation was performed using a Shim-pack XR-ODS (3.0 x 50 mm, 2.2 mm) column with an oven temperature of 35°C. The mobile phase comprised of water with 0.1 % formic acid (A) and acetonitrile with 0.1% formic acid (B). A binary gradient elution of 0.0-3.0 min 5 % B, 10.0 min 20 % B, 10.1 min 50 % B, 13.0 min 50 % B, 13.1 min 5% B, 20.0 min 5 % B, at a flow rate of 0.5 mL/min. High resolution mass spectrometric (HRMS) data was measure using an electrospray ionisation (ESI) probe with a CDL and a heat block temperature of 200°C, and an N_2 nebulising gas flow rate of 1.5 L/min. Data acquisition was performed in both positive and negative ionisation with polarity switching. A positive acquisition range of 100-1000 m/z with ion accumulation at 5.0 msec, and a negative acquisition range of 200-1000 m/z with ion accumulation at 2.0 msec. Samples were held in the autosampler at 5 °C whilst queued for analysis. The LCMS-IT-TOF mass accuracy was calibrated with sodium trifluoroacetate clusters prior to analysis of the batch of samples. LCMS data was analysed using Shimadzu LCMSsolution software, peak areas were calculated for the predicted m/z value of $[M+H]^+$ ion and $[M-H]^-$ ions in positive and negative ionisation scan modes respectively, using the Qualitative Peak Integration function in the LCMS Postrun Analysis software.

Binding of heparin to apoA-I fibrils: *In vitro* binding assays of apoA-I fibril-heparin binding were performed using an adaptation of a procedure described previously (82), in which the amount of GAG remaining unbound at different fibril:GAG concentration ratios was determined using *Bacteroides* heparinase I (New England Biolabs (UK) Ltd). The heparinase enzyme cleaves heparin yielding oligosaccharide products containing unsaturated uronic acids, which can be detected using UV spectroscopy at 232 nm. Fibrils were prepared by acidification of apoA-I in the presence of heparin (Sigma), at the following protein/heparin molar ratios: 1:0.5, 1:1 and 1:2. In addition samples of protein only and heparin only were prepared as controls. In all cases the heparin concentration was kept at 1 mg/ml (72 μM). ApoA-I was initially solubilized in pH 7 McIlvaine's buffer together with heparin before carrying out a shift to pH 4 with the addition of concentrated HCl. Samples were incubated at 37 °C for 3 d with shaking to allow fibril formation prior to sedimentation of the protein. The supernatant was removed and returned to pH 7 with 5M NaOH before assay. Samples were monitored at 30 °C, with A_{232} measurements taken every 10 s until maximal absorbance was reached. The amount of heparin remaining in solution was then calculated from a heparin calibration curve.

Effect of green tea compounds on the aggregation of apoA-I: ThT fluorescence experiments were carried out as described in ref (12). Briefly, apoA-I (7.2 μM) was incubated with ThT alone and in the presence of 14.4 μM heparin. Samples (in triplicate) were incubated with no further additives, or with pure green tea extract solution (6.6 ng/mL, roughly equivalent to a 2-fold molar excess of EGCG) or 14.4 μM EGCG. After measuring the fluorescence for 10 minutes, concentrated HCl was added to reduce the sample to pH 4 and induce aggregation. ThT fluorescence measurements were taken over 300 minutes at 1 min intervals.

Binding of EGCG to apoA-I fibrils: ApoA-I (36 μM) was incubated alone or with increasing concentrations of EGCG at pH 4, 37°C for 3 d with agitation. After this time, the fibrils of apoA-I formed in the absence of EGCG were incubated for a further 24 h in the presence of EGCG. The insoluble material was removed by centrifugation at 13,400 rpm in a bench-top centrifuge. The absorbance of the supernatant at 274 nm (the wavelength of maximum absorption of EGCG) was measured and used to determine how much EGCG remained in solution by comparison with a standard curve of A_{274} for

EGCG at a range of concentrations from 0.01 mM to 1 mM.

Transmission electron microscopy: ApoA-I (36 μM), in the absence and presence of heparin (72 μM), was incubated at pH 4, 37°C with agitation for 3 days. Samples were centrifuged and the pellets washed several times with distilled water to remove buffer salts. Some pellets were resuspended in 36 μM EGCG and incubated overnight at 25°C before removal of the bulk solution by centrifugation. Pellets were then diluted to 18 μM, before 10 μL was loaded onto carbon-coated copper grids and incubated for 30 s. Excess sample was removed by blotting. Grids (Agar Scientific Ltd., Stansted, UK) were washed with 2 x 10 μL water. The grid was then stained by inverting it onto a 10 μL droplet of 2 % (w/v) uranyl acetate and blotting, followed by addition of another 10 μL uranyl acetate droplet. After 30 seconds of staining, the grid was blotted and left to dry for 5 minutes at room temperature. The sample was then visualised on a JEOL JEM-1400 electron microscope at 100 kV. TEM images were calibrated in ImageJ (NIH) using the TEM scale bar on each image. Calibrated lines were drawn to measure fibril width for a total of 25 instances per image. These instances could include up to three measurements of the same fibril at different positions in the image. A total of five images for ApoA alone and five images of ApoA + heparin were analyzed, resulting in an average fibril width of 10.7 nm ± 0.4 nm for ApoA alone and 15.4 nm ± 1.3 nm for ApoA + heparin. All measurements were then binned into 1 nm categories for data presentation.

Circular dichroism spectroscopy: ApoA-I (36 μM) alone or in the presence of heparin (72 μM) was incubated at pH 4, 37 °C for 3 d with agitation. The samples were centrifuged and the pellets washed several times with distilled water to remove buffer salts. The aggregated apoA-I was resuspended in McIlvaine buffer, or McIlvaine buffer containing 36 μM EGCG. The samples were then incubated at 37 °C with agitation for 24 hours and then centrifuged at 14,000 rpm to remove the insoluble aggregated protein. Spectra of the supernatants were acquired on a Chirascan Plus CD spectrometer between 180 and 260 nm with a bandwidth of 1 nm, using a path length of 0.2 mm. Background signals (i.e. from buffer, heparin, EGCG or EGCG and heparin) were subtracted and the spectra were analysed using CDApps software (83). Fitting was performed using the CONTINLL algorithm.

Dynamic Light Scattering: ApoA-I (36 μM) in the absence and presence of heparin (72 μM) was incubated at pH 4, 37°C with agitation for 3 days. Insoluble fibrils were centrifuged and washed 3 times with distilled water to remove buffer salts. The fibrils were resuspended in McIlvaine buffer, or McIlvaine buffer with 36 μM EGCG and incubated at 37°C for 24 hours. The insoluble aggregated material was removed through centrifugation at 14,000 rpm, and the supernatant loaded into low volume plastic cuvettes. DLS spectra were acquired on a Zetasizer Nano Zs instrument. The size distribution (nm) by percentage volume was recorded and averaged over 3 scans.

Solid-state NMR: Uniformly ^{13}C-labelled apoA-I (5 mg at 36 μM) was incubated with agitation at pH 4, 37°C for 3 d alone or in the presence of 72 M heparin or with 72 μM heparin and 36 μM EGCG. Following the production of insoluble material, aggregates were harvested by centrifugation at 12,000 g for 10 minutes. The aggregates were centrifuged into a zirconium 3.2 mm rotor with a Kel-F cap (Bruker, U.K). In some samples EGCG (36 μM) was added in a volume of 5 mL to the apoA-I samples and left for 24 hours before transferring the pellet to the NMR rotor.

Two-dimensional ^{13}C-^{13}C SSNMR spectra were recorded at a magnetic field of 16.3 Tesla on a Bruker Avance III 700 spectrometer, with a 3.2 mm HXY probe operating in double resonance mode. Spectra were obtained with magic angle spinning at 14 kHz. Hartmann-Hahn cross-polarization was achieved with a 2 ms contact time, and 100 kHz proton decoupling with SPINAL-64 applied during signal acquisition. During the mixing time of 20 ms, the ^{1}H nutation frequency was lowered to 14 kHz, to achieve dipolar-assisted rotational resonance (DARR) mixing. A total of 256 t_1 increments were recorded using the States-TPPI method for phase sensitivity, with 256 transients per

increment. One and two-dimensional refocused INEPT SSNMR spectra (84) and proton-decoupled ^{15}N cross-polarisation magic-angle spinning (CP-MAS) spectra were recorded at a magnetic field of 9.3 Tesla on a Bruker Avance III 400 spectrometer. Spectra were obtained with magic-angle spinning at 8 kHz. For CP-MAS, a contact time of 2 ms and proton spin-lock frequency of 63 kHz were applied, with proton decoupling at 83 kHz.

Solution-state NMR: Proton spectra were recorded at a magnetic field of 9.3 Tesla. Spectra were obtained for EGCG (360 µM) in 10 mM phosphate buffer, pH 7, alone or in the presence of heparin (36 µM) or apoA-I (36 µM). 1D gradient NOESY experiments were acquired with relaxation delays of 2 s, a mixing time of 10 ms, a presaturation power of 25 Hz and 128 scans. Gradient strengths were the default for this sequence: GPZ1 50%, GPZ2 -10%. Spectral width was 8012.82 Hz, the offset on-resonance with the water peak, and 64k points (acquisition time 4.1 s). Spectra were zero-filled once and processed with a 0.3 Hz exponential line-broadening. WaterLOGSY spectra were acquired with relaxation delays of 1 s, a mixing time of 1.7 s, 2 dummy scans and 128 scans. No spin-lock was applied in order to observe the receptor signals. The selective inversion pulse for the NOESY block was a 7.5 ms Gaussian pulse, while that in the excitation sculpting block was a 2 ms sinc pulse (again, the prosol defaults). The spectral width was 6393.862 Hz, the offset on-resonance with the water peak, and 16 k points (acquisition time 1.28 s). Spectra were zero-filled once and processed with a 1 Hz exponential line-broadening.

Cell Viability: Human umbilical artery endothelial cells (HUAEC) (Sigma) were plated on 96 well plates at a cell density of ~ 5000 cells per well and grown over night at 37 °C to allow the cells to adhere. ApoA-1 aggregates (72 µM) were formed over 3 days at pH 4 in the presence or absence of 144 µM heparin. Fibrils were pelleted and washed x3 in pH 4 McIlvaine's to remove any unaggregated material, before re-suspending at the same concentrations. Samples were divided in to equal volume aliquots and EGCG added at a range of concentrations to give molar ratios of 0, 0.1, 0.2, 0.5, 1, 2 and 5:1 EGCG: apoA-1, and left for a further 24 h, before the addition of 10 µl samples to the cells (100 µl assay volume). Following incubation at 37 °C for 48 h, 10 µl of the Cell Counting Kit (CCK-8) (Sigma), solution was added and incubated for a further 3 h prior to absorbance measurement at 450 nm.

Acknowledgments

Funding was provided by the British Heart Foundation (FS/13/28/30208 and PG/16/97/32567). EH and KLS were funded by BBSRC (BB/K01451X/1 and BB/K015958/1). SER also acknowledges funding from the European Research Council (ERC) under European Union's Seventh Framework Programme (FP7/2007-2013) ERC grant agreement no. 322408 and the Wellcome Trust (089311/Z/09/Z). We thank Dr Michael Oda for the gift of the apoA-I expression clone, Mr Mark Blandamer for technical assistance with the chromatographic analysis of green tea extracts and Dr Mike Coogan for assistance with fluorescence lifetime imaging.

Conflict of interest

The authors declare that they have no conflicts of interest with the contents of this article.

References

1. Sipe, J. D., Benson, M. D., Buxbaum, J. N., Ikeda, S.-i., Merlini, G., Saraiva, M. J. M., and Westermark, P. (2012) Amyloid fibril protein nomenclature: 2012 recommendations from the Nomenclature Committee of the International Society of Amyloidosis. *Amyloid-Journal of Protein Folding Disorders* **19**, 167-170
2. Raimondi, S., Guglielmi, F., Giorgetti, S., Di Gaetano, S., Arciello, A., Monti, D. M., Relini, A., Nichino, D., Doglia, S. M., Natalello, A., Pucci, P., Mangione, P., Obici, L., Merlini, G., Stoppini, M., Robustelli, P., Gaetano Tartaglia, G., Vendruscolo, M., Dobson, C. M., Piccoli, R., and Bellotti, V. (2011) Effects of the Known Pathogenic Mutations on the Aggregation Pathway of the Amyloidogenic Peptide of Apolipoprotein A-I. *J. Mol. Biol.* **407**, 465-476
3. Rowczenio, D., Dogan, A., Theis, J. D., Vrana, J. A., Lachmann, H. J., Wechalekar, A. D., Gilbertson, J. A., Hunt, T., Gibbs, S. D. J., Sattianayagam, P. T., Pinney, J. H., Hawkins, P. N., and Gillmore, J. D. (2011) Amyloidogenicity and Clinical Phenotype Associated with Five Novel Mutations in Apolipoprotein A-I. *Am. J. Pathol.* **179**, 1978-1987
4. Westermark, P., Mucchiano, G., Marthin, T., Johnson, K. H., and Sletten, K. (1995) Apolipoprotein A1-Derived Amyloid in Human Aortic Atherosclerotic Plaques. *Am. J. Pathol.* **147**, 1186-1192
5. Obici, L., Franceschini, G., Calabresi, L., Giorgetti, S., Stoppini, M., Merlini, G., and Bellotti, V. (2006) Structure, function and amyloidogenic propensity of apolipoprotein A-1. *Amyloid-Journal of Protein Folding Disorders* **13**, 191-205
6. Rocken, C., Tautenhahn, J. R., Buhling, F., Sachwitz, D., Vockler, S., Goette, A., and Burger, T. (2006) Prevalence and pathology of amyloid in atherosclerotic arteries. *Arteriosclerosis Thrombosis and Vascular Biology* **26**, 676-677
7. Mucchiano, G. I., Jonasson, L., Haggqvist, B., Einarsson, E., and Westermark, P. (2001) Apolipoprotein A-I-derived amyloid in atherosclerosis - Its association with plasma levels of apolipoprotein A-I and cholesterol. *Am. J. Clin. Pathol.* **115**, 298-303
8. Chiti, F., and Dobson, C. M. (2006) Protein misfolding, functional amyloid, and human disease. in *Annu. Rev. Biochem.* pp 333-366
9. Mucchiano, G. I., Haggqvist, B., Sletten, K., and Westermark, P. (2001) Apolipoprotein A-I-derived amyloid in atherosclerotic plaques of the human aorta. *J. Pathol.* **193**, 270-275
10. Ramella, N. A., Schinella, G. R., Ferreira, S. T., Prieto, E. D., Vela, M. E., Luis Rios, J., Alejandra Tricerri, M., and Rimoldi, O. J. (2012) Human Apolipoprotein A-I Natural Variants: Molecular Mechanisms Underlying Amyloidogenic Propensity. *PLoS One* **7**
11. Ramella, N. A., Rimoldi, O. J., Prieto, E. D., Schinella, G. R., Sanchez, S. A., Jaureguiberry, M. S., Vela, M. E., Ferreira, S. T., and Alejandra Tricerri, M. (2011) Human Apolipoprotein A-I-Derived Amyloid: Its Association with Atherosclerosis. *PLoS One* **6**
12. Townsend, D., Hughes, E., Hussain, R., Siligardi, G., Baldock, S., Madine, J., and Middleton, D. A. (2017) Heparin and Methionine Oxidation Promote the Formation of Apolipoprotein A-I Amyloid Comprising alpha-Helical and beta-Sheet Structures. *Biochemistry* **56**, 1632-1644
13. Wong, Y. Q., Binger, K. J., Howlett, G. J., and Griffin, M. D. W. (2010) Methionine oxidation induces amyloid fibril formation by full-length apolipoprotein A-I. *Proc. Natl. Acad. Sci. U. S. A.* **107**, 1977-1982
14. Naghavi, M., John, R., Naguib, S., Siadaty, M. S., Grasu, R., Kurian, K. C., van Winkle, W. B., Soller, B., Litovsky, S., Madjid, M., Willerson, J. T., and Casscells, W. (2002) pH heterogeneity of human and rabbit atherosclerotic plaques; a new insight into detection of vulnerable plaque. *Atherosclerosis* **164**, 27-35
15. Alexandrescu, A. T. (2005) Amyloid accomplices and enforcers. *Protein Sci.* **14**, 1-12
16. Kisilevsky, R., Ancsin, J. B., Szarek, W. A., and Petanceska, S. (2007) Heparan sulfate as a therapeutic target in amyloidogenesis: prospects and possible complications (vol 14, pg 21, 2007). *Amyloid-Journal of Protein Folding Disorders* **14**
17. McLaurin, J., Franklin, T., Zhang, X. Q., Deng, J. P., and Fraser, P. E. (1999) Interactions of Alzheimer amyloid-beta peptides with glycosaminoglycans - effects on fibril nucleation and growth. *Eur. J. Biochem.* **266**, 1101-1110

18. Motamedi-Shad, N., Monsellier, E., Torrassa, S., Relini, A., and Chiti, F. (2009) Kinetic analysis of amyloid formation in the presence of heparan sulfate: faster unfolding and change of pathway. *J. Biol. Chem.* **284**, 29921-29934
19. Valle-Delgado, J. J., Alfonso-Prieto, M., de Groot, N. S., Ventura, S., Samitier, J., Rovira, C., and Fernandez-Busquets, X. (2010) Modulation of A-beta42 fibrillogenesis by glycosaminoglycan structure. *FASEB J.* **24**, 4250-4261
20. Guptabansal, R., Frederickson, R. C. A., and Brunden, K. R. (1995) Proteoglycan-mediated inhibition of A-beta proteolysis - a potential cause of senile plaque accumulation. *J. Biol. Chem.* **270**, 18666-18671
21. Bravo, R., Arimon, M., Valle-Delgado, J. J., Garcia, R., Durany, N., Castel, S., Cruz, M., Ventura, S., and Fernandez-Busquets, X. (2008) Sulfated polysaccharides promote the assembly of amyloid beta(1-42) peptide into stable fibrils of reduced cytotoxicity. *J. Biol. Chem.* **283**, 32471-32483
22. Pollack, S. J., Sadler, I. I. J., Hawtin, S. R., Tailor, V. J., and Shearman, M. S. (1995) Sulfated glycosaminoglycans and dyes attenuate the neurotoxic effects of beta-amyloid in rat PC12 cells. *Neurosci. Lett.* **184**, 113-116
23. O'Brien, K. D., Olin, K. L., Alpers, C. E., Chiu, W., Ferguson, M., Hudkins, K., Wight, T. N., and Chait, A. (1998) Comparison of apolipoprotein and proteoglycan deposits in human coronary atherosclerotic plaques - Colocalization of biglycan with apolipoproteins. *Circulation* **98**, 519-527
24. de Pascual-Teresa, S., Moreno, D. A., and Garcia-Viguera, C. (2010) Flavanols and Anthocyanins in Cardiovascular Health: A Review of Current Evidence. *Int. J. Mol. Sci.* **11**, 1679-1703
25. Peter, B., Bosze, S., and Horvath, R. (2017) Biophysical characteristics of proteins and living cells exposed to the green tea polyphenol epigallocatechin-3-gallate (EGCg): review of recent advances from molecular mechanisms to nanomedicine and clinical trials. *European Biophysics Journal with Biophysics Letters* **46**, 1-24
26. Engel, M. F. M., VandenAkker, C. C., Schleeger, M., Velikov, K. P., Koenderink, G. H., and Bonn, M. (2012) The Polyphenol EGCG Inhibits Amyloid Formation Less Efficiently at Phospholipid Interfaces than in Bulk Solution. *J. Am. Chem. Soc.* **134**, 14781-14788
27. Wang, Q. Q., Guo, J. J., Jiao, P. Z., Liu, H. X., and Yao, X. J. (2014) Exploring the Influence of EGCG on the beta-Sheet-Rich Oligomers of Human Islet Amyloid Polypeptide (hIAPP(1-37)) and Identifying Its Possible Binding Sites from Molecular Dynamics Simulation. *PLoS One* **9**
28. Ehrnhoefer, D. E., Bieschke, J., Boeddrich, A., Herbst, M., Masino, L., Lurz, R., Engemann, S., Pastore, A., and Wanker, E. E. (2008) EGCG redirects amyloidogenic polypeptides into unstructured, off-pathway oligomers. *Nat. Struct. Mol. Biol.* **15**, 558-566
29. Bieschke, J., Russ, J., Friedrich, R. P., Ehrnhoefer, D. E., Wobst, H., Neugebauer, K., and Wanker, E. E. (2010) EGCG remodels mature alpha-synuclein and amyloid-beta fibrils and reduces cellular toxicity. *Proc. Natl. Acad. Sci. U. S. A.* **107**, 7710-7715
30. Huang, R., Vivekanandan, S., Brender, J. R., Abe, Y., Naito, A., and Ramamoorthy, A. (2012) NMR Characterization of Monomeric and Oligomeric Conformations of Human Calcitonin and Its Interaction with EGCG. *J. Mol. Biol.* **416**, 108-120
31. Ahmed, R., VanSchouwen, B., Jafari, N., Ni, X. D., Ortega, J., and Melacini, G. (2017) Molecular Mechanism for the (-)-Epigallocatechin Gallate-Induced Toxic to Nontoxic Remodeling of A beta Oligomers. *J. Am. Chem. Soc.* **139**, 13720-13734
32. Hyung, S. J., DeToma, A. S., Brender, J. R., Lee, S., Vivekanandan, S., Kochi, A., Choi, J. S., Ramamoorthy, A., Ruotolo, B. T., and Lim, M. H. (2013) Insights into antiamyloidogenic properties of the green tea extract (-)-epigallocatechin-3-gallate toward metal-associated amyloid-beta species. *Proc. Natl. Acad. Sci. U. S. A.* **110**, 3743-3748
33. Palhano, F. L., Lee, J., Grimster, N. P., and Kelly, J. W. (2013) Toward the Molecular Mechanism(s) by Which EGCG Treatment Remodels Mature Amyloid Fibrils. *J. Am. Chem. Soc.* **135**, 7503-7510
34. Mereles, D., and Hunstein, W. (2011) Epigallocatechin-3-gallate (EGCG) for Clinical Trials: More Pitfalls than Promises? *Int. J. Mol. Sci.* **12**, 5592-5603

35. Naumovski, N., Blades, B. L., and Roach, P. D. (2015) Food Inhibits the Oral Bioavailability of the Major Green Tea Antioxidant Epigallocatechin Gallate in Humans. *Antioxidants* **4**, 373-393
36. Nakajima, H., Nishitsuji, K., Kawashima, H., Kuwabara, K., Mikawa, S., Uchimura, K., Akaji, K., Kashiwada, Y., Kobayashi, N., Saito, H., and Sakashita, N. (2016) The polyphenol (-)-epigallocatechin-3-gallate prevents apoA-I-Iowa amyloidosis in vitro and protects human embryonic kidney 293 cells against amyloid cytotoxicity. *Amyloid-Journal of Protein Folding Disorders* **23**, 17-25
37. Ren, R. Y., Hong, Z. N., Gong, H. Y., Laporte, K., Skinner, M., Seldin, D. C., Costello, C. E., Connors, L. H., and Trinkaus-Randall, V. (2010) Role of Glycosaminoglycan Sulfation in the Formation of Immunoglobulin Light Chain Amyloid Oligomers and Fibrils. *J. Biol. Chem.* **285**, 37672-37682
38. Wang, H., Cao, P., and Raleigh, D. P. (2013) Amyloid Formation in Heterogeneous Environments: Islet Amyloid Polypeptide Glycosaminoglycan Interactions. *J. Mol. Biol.* **425**, 492-505
39. Snow, A. D., Mar, H., Nochlin, D., Sekiguchi, R. T., Kimata, K., Koike, Y., and Wight, T. N. (1990) Early accumulation of heparan sulfate in neurons and in the beta-amyloid protein-containing lesions of Alzheimer's disease and Down's syndrome. *Am. J. Pathol.* **137**, 1253-1270
40. van Horssen, J., Wesseling, P., van den Heuvel, L., de Waal, R. M. W., and Verbeek, M. M. (2003) Heparan sulphate proteoglycans in Alzheimer's disease and amyloid-related disorders. *Lancet Neurol.* **2**, 482-492
41. Castillo, G. M., Lukito, W., Wight, T. N., and Snow, A. D. (1999) The sulfate moieties of glycosaminoglycans are critical for the enhancement of beta-amyloid protein fibril formation. *J. Neurochem.* **72**, 1681-1687
42. Stewart, K. L., Hughes, E., Yates, E. A., Middleton, D. A., and Radford, S. E. (2017) Molecular Origins of the Compatibility between Glycosaminoglycans and A beta 40 Amyloid Fibrils. *J. Mol. Biol.* **429**, 2449-2462
43. Lopez del Amo, J. M., Fink, U., Dasari, M., Grelle, G., Wanker, E. E., Bieschke, J., and Reif, B. (2012) Structural Properties of EGCG-Induced, Nontoxic Alzheimer's Disease A beta Oligomers. *J. Mol. Biol.* **421**, 517-524
44. Kristen, A. V., Lehrke, S., Buss, S., Mereles, D., Steen, H., Ehlermann, P., Hardt, S., Giannitsis, E., Schreiner, R., Haberkorn, U., Schnabel, P. A., Linke, R. P., Roecken, C., Wanker, E. E., Dengler, T. J., Altland, K., and Katus, H. A. (2012) Green tea halts progression of cardiac transthyretin amyloidosis: an observational report. *Clin. Res. Cardiol.* **101**, 805-813
45. Stewart, K. L., Hughes, E., Yates, E. A., Akien, G. R., Huang, T. Y., Lima, M. A., Rudd, T. R., Guerrini, M., Hung, S. C., Radford, S. E., and Middleton, D. A. (2016) Atomic Details of the Interactions of Glycosaminoglycans with Amyloid-beta Fibrils. *J. Am. Chem. Soc.* **138**, 8328-8331
46. Sang, S. M., Lee, M. J., Hou, Z., Ho, C. T., and Yang, C. S. (2005) Stability of tea polyphenol (-)-epigallocatechin-3-gallate and formation of dimers and epimers under common experimental conditions. *J. Agric. Food. Chem.* **53**, 9478-9484
47. Ishii, T., Mori, T., Tanaka, T., Mizuno, D., Yamaji, R., Kumazawa, S., Nakayama, T., and Akagawa, M. (2008) Covalent modification of proteins by green tea polyphenol (-)-epigallocatechin-3-gallate through autoxidation. *Free Radical Biol. Med.* **45**, 1384-1394
48. Mizooku, Y., Yoshikawa, M., Tsuneyoshi, T., and Arakawa, R. (2003) Analysis of oxidized epigallocatechin gallate by liquid chromatography/mass spectrometry. *Rapid Commun. Mass Spectrom.* **17**, 1915-1918
49. Dragicevic, N., Smith, A., Lin, X. Y., Yuan, F., Copes, N., Delic, V., Tan, J., Cao, C. H., Shytle, R. D., and Bradshaw, P. C. (2011) Green Tea Epigallocatechin-3-Gallate (EGCG) and Other Flavonoids Reduce Alzheimer's Amyloid-Induced Mitochondrial Dysfunction. *Journal of Alzheimers Disease* **26**, 507-521
50. Rezai-Zadeh, K., Arendash, G. W., Hou, H. Y., Fernandez, F., Jensen, M., Runfeldt, M., Shytle, R. D., and Tan, J. (2008) Green tea epigallocatechin-3-gallate (EGCG) reduces beta-

amyloid mediated cognitive impairment and modulates tau pathology in Alzheimer transgenic mice. *Brain Res.* **1214**, 177-187

51. Attar, A., Rahimi, F., and Bitan, G. (2013) Modulators of amyloid protein aggregation and toxicity: EGCG and CLR01. *Transl. Neurosci.* **4**, 385-409
52. Stenvang, M., Christiansen, G., and Otzen, D. E. (2016) Epigallocatechin Gallate Remodels Fibrils of Lattice Corneal Dystrophy Protein, Facilitating Proteolytic Degradation and Preventing Formation of Membrane-Permeabilizing Species. *Biochemistry* **55**, 2344-2357
53. Meng, F. L., Abedini, A., Plesner, A., Verchere, C. B., and Raleigh, D. P. (2010) The Flavanol (-)-Epigallocatechin 3-Gallate Inhibits Amyloid Formation by Islet Amyloid Polypeptide, Disaggregates Amyloid Fibrils, and Protects Cultured Cells against IAPP-Induced Toxicity. *Biochemistry* **49**, 8127-8133
54. Ehrnhoefer, D. E., Duennwald, M., Markovic, P., Wacker, J. L., Engemann, S., Roark, M., Legleiter, J., Marsh, J. L., Thompson, L. M., Lindquist, S., Muchowski, P. J., and Wanker, E. E. (2006) Green tea (-)-epigallocatechin-gallate modulates early events in huntingtin misfolding and reduces toxicity in Huntington's disease models. *Hum. Mol. Genet.* **15**, 2743-2751
55. Ferreira, N., Saraiva, M. J., and Almeida, M. R. (2011) Natural polyphenols inhibit different steps of the process of transthyretin (TTR) amyloid fibril formation. *FEBS Lett.* **585**, 2424-2430
56. Cohlberg, J. A., Li, J., Uversky, V. N., and Fink, A. L. (2002) Heparin and other glycosaminoglycans stimulate the formation of amyloid fibrils from alpha-synuclein in vitro. *Biochemistry* **41**, 1502-1511
57. Jha, S., Patil, S. M., Gibson, J., Nelson, C. E., Alder, N. N., and Alexandrescu, A. T. (2011) Mechanism of Amylin Fibrillization Enhancement by Heparin. *J. Biol. Chem.* **286**, 22894-22904
58. Watson, D. J., Lander, A. D., and Selkoe, D. J. (1997) Heparin-binding properties of the amyloidogenic peptides A beta and amylin - Dependence on aggregation state and inhibition by Congo red. *J. Biol. Chem.* **272**, 31617-31624
59. Madine, J., Pandya, M. J., Hicks, M. R., Rodger, A., Yates, E. A., Radford, S. E., and Middleton, D. A. (2012) Site-Specific Identification of an A ss Fibril-Heparin Interaction Site by Using Solid-State NMR Spectroscopy. *Angewandte Chemie-International Edition* **51**, 13140-13143
60. Malmos, K. G., Bjerring, M., Jessen, C. M., Nielsen, E. H. T., Poulsen, E. T., Christiansen, G., Vosegaard, T., Skrydstrup, T., Enghild, J. J., Pedersen, J. S., and Otzen, D. E. (2016) How Glycosaminoglycans Promote Fibrillation of Salmon Calcitonin. *J. Biol. Chem.* **291**, 16849-+
61. Mamos, K. G., Stenvang, M., Sahinl, C., Christiansen, G., and Otzen, D. E. (2017) The Changing Face of Aging: Highly Sulfated Glycosaminoglycans Induce Amyloid Formation in a Lattice Corneal Dystrophy Model Protein. *J. Mol. Biol.* **429**, 2755-2764
62. Vitello, L. B., and Scanu, A. M. (1976) Studies on human-serum high-density lipoproteins - self association of apolipoprotein A-I in aqueous solutions *J. Biol. Chem.* **251**, 1131-1136
63. Zhao, J., Liang, Q. N., Sun, Q., Chen, C. H., Xu, L. H., Ding, Y., and Zhou, P. (2017) (-)-Epigallocatechin-3-gallate (EGCG) inhibits fibrillation, disaggregates amyloid fibrils of alpha-synuclein, and protects PC12 cells against alpha-synuclein-induced toxicity. *Rsc Advances* **7**, 32508-32517
64. Mei, X. H., and Atkinson, D. (2011) Crystal Structure of C-terminal Truncated Apolipoprotein A-I Reveals the Assembly of High Density Lipoprotein (HDL) by Dimerization. *J. Biol. Chem.* **286**, 38570-38582
65. Bibow, S., Polyhach, Y., Eichmann, C., Chi, C. N., Kowal, J., Albiez, S., McLeod, R. A., Stahlberg, H., Jeschke, G., Guntert, P., and Riek, R. (2017) Solution structure of discoidal high-density lipoprotein particles with a shortened apolipoprotein A-I. *Nat. Struct. Mol. Biol.* **24**, 187-+
66. Vilasi, S., Sarcina, R., Maritato, R., De Simone, A., Irace, G., and Sirangelo, I. (2011) Heparin Induces Harmless Fibril Formation in Amyloidogenic W7FW14F Apomyoglobin and Amyloid Aggregation in Wild-Type Protein In Vitro. *PLoS One* **6**, 13

67. Galzitskaya, O. V., and Selivanova, O. M. (2017) Rosetta Stone for Amyloid Fibrils: The Key Role of Ring-Like Oligomers in Amyloidogenesis. *Journal of Alzheimers Disease* **59**, 785-795
68. Chan, G. K. L., Witkowski, A., Gantz, D. L., Zhang, T. Q. O., Zanni, M. T., Jayaraman, S., and Cavigiolio, G. (2015) Myeloperoxidase-mediated Methionine Oxidation Promotes an Amyloidogenic Outcome for Apolipoprotein A-I. *J. Biol. Chem.* **290**, 10958-10971
69. Lorenzen, N., Nielsen, S. B., Yoshimura, Y., Vad, B. S., Andersen, C. B., Betzer, C., Kaspersen, J. D., Christiansen, G., Pedersen, J. S., Jensen, P. H., Mulder, F. A. A., and Otzen, D. E. (2014) How Epigallocatechin Gallate Can Inhibit alpha-Synuclein Oligomer Toxicity in Vitro. *J. Biol. Chem.* **289**, 21299-21310
70. Manach, C., Williamson, G., Morand, C., Scalbert, A., and Remesy, C. (2005) Bioavailability and bioefficacy of polyphenols in humans. I. Review of 97 bioavailability studies. *Am. J. Clin. Nutr.* **81**, 230S-242S
71. Eaton, J. D., and Williamson, M. P. (2017) Multi-site binding of epigallocatechin gallate to human serum albumin measured by NMR and isothermal titration calorimetry. *Biosci. Rep.* **37**
72. Bratzler, R. L., Chisolm, G. M., Colton, C. K., Smith, K. A., Zilversmit, D. B., and Lees, R. S. (1977) Distribution of labeled albumin across rabbit thoracic aorta in vivo. *Circul. Res.* **40**, 182-190
73. Smith, E. B., and Staples, E. M. (1980) DISTRIBUTION OF PLASMA-PROTEINS ACROSS THE HUMAN AORTIC-WALL - BARRIER FUNCTIONS OF ENDOTHELIUM AND INTERNAL ELASTIC LAMINA. *Atherosclerosis* **37**, 579-590
74. Li, M., and Hagerman, A. E. (2014) Role of the Flavan-3-ol and Galloyl Moieties in the Interaction of (-)-Epigallocatechin Gallate with Serum Albumin. *J. Agric. Food. Chem.* **62**, 3768-3775
75. Fraser, P. E., Darabie, A. A., and McLaurin, J. (2001) Amyloid-beta interactions with chondroitin sulfate-derived monosaccharides and disaccharides: Implications for drug development. *J. Biol. Chem.* **276**, 6412-6419
76. Dewitt, D. A., Silver, J., Canning, D. R., and Perry, G. (1993) Chondroitin sulfate proteoglycans are associated with the lesions of Alzheimer's disease. *Exp. Neurol.* **121**, 149-152
77. Zhang, Z., Ohtake-Niimi, S., Kadomatsu, K., and Uchimura, K. (2016) Reduced molecular size and altered disaccharide composition of cerebral chondroitin sulfate upon Alzheimer's pathogenesis. *Glycobiology* **26**, 1443-1443
78. Snow, A. D., Mar, H., Nochlin, D., Kresse, H., and Wight, T. N. (1992) Peripheral distribution of dermatan sulfate proteoglycans (decorin) in amyloid-containing plaques and their presence in neurofibrillary tangles of Alzheimer's disease. *J. Histochem. Cytochem.* **40**, 105-113
79. Snow, A. D., Nochlin, D., Sekiguchi, R., and Carlson, S. S. (1996) Identification and immunolocalization of a new class of proteoglycan (keratan sulfate) to the neuritic plaques of Alzheimer's disease. *Exp. Neurol.* **138**, 305-317
80. Ryan, R. O., Forte, T. M., and Oda, M. N. (2003) Optimized bacterial expression of human apolipoprotein A-I. *Protein Expression Purif.* **27**, 98-103
81. Oda, M. N., Bielicki, J. K., Berger, T., and Forte, T. M. (2001) Cysteine substitutions in apolipoprotein A-I primary structure modulate paraoxonase activity. *Biochemistry* **40**, 1710-1718
82. Madine, J., Pandya, M. J., Hicks, M. R., Rodger, A., Yates, E. A., Radford, S. E., and Middleton, D. A. (2012) Site-specific identification of an A-beta fibril-heparin interaction site by using solid-state NMR spectroscopy. *Angew. Chemie. Int. Ed.* **51**, 13140-13143
83. Hussain, R., Benning, K., Javorfi, T., Longo, E., Rudd, T. R., Pulford, B., and Siligardi, G. (2015) CDApps: integrated software for experimental planning and data processing at beamline B23, Diamond Light Source. *Journal of Synchrotron Radiation* **22**, 465-468
84. Elena, B., Lesage, A., Steuernagel, S., Bockmann, A., and Emsley, L. (2005) Proton to carbon-13 INEPT in solid-state NMR spectroscopy. *J. Am. Chem. Soc.* **127**, 17296-17302

Footnotes

The abbreviations used are: Aβ, amyloid-beta; Aβ40, amyloid beta (1-40); AL, antibody light chain; ApoA-I, aplipoprotein A-I; CD, circular dichroism; DARR, dipole-assisted rotational resonance; DLS, dynamic light scattering; ECG, epicathin-3-gallate; EGCG, epigallocathin-3-gallate; GAG, glycosaminoglycan; HDL, high density lipoprotein; HPLC, high-performance liquid chromatography; HUAEC, human umbilical artery endothelial cells; INEPT, insensitive nuclei enhanced by polarization transfer; MAS, magic angle spinning; NMR, nuclear magnetic resonance; ssNME, solid state nuclear magnetic resonance; TEM, transmission electron microscopy; ThT, Thioflavin-T; TSP, trimethylsilylpropanoate.

Table 1. ApoA-I fibril binding of microwave-extracted green tea catechins as quantified from the HPLC peak intensities. Fibrils formed from 36 μM apoA-I were centrifuged and resuspended in 200 ml green tea extract solution before further centrifugation and HPLC analysis of the supernatant.

	Concentration		
Compound	Initial (μg/ml)[a]	Bound (μg/ml)[b]	Bound (%)
1. Gallocatechin	337.1	7.3	2.2
2. Catechin	506.4	46.0	9.1
3. Caffeine	302.9	62.6	20.7
4. Epicatechin	154.9	0	0
5. Epigallocatechin-3-gallate	958.7	533.2	55.6
6. Gallocatechin-3-gallate[c]	35.2	24.8	70.6
7. Epicatechin-3-gallate	200.3	98.0	48.9
8. Catechin-3- gallate[c]	52.7	9.7	18.5

[a]Initial concentrations before addition of fibrils were estimated from a peak-by-peak comparison of the HPLC chromatograms of the microwave extracted solution and the standard green tea solution.

[b]Bound concentrations are given as the initial concentrations minus the supernatant concentrations after addition and sedimentation of the fibrils.

[c]Approximate values only, as concentrations too low to measure accurately.

Table 2. Measured chemical shifts from the ^{1}H-^{13}C INEPT SSNMR spectrum of apoA-I fibrils treated with EGCG and mean predicted chemical shifts for the given amino acids in α-helical and β-sheet environments. Chemical shifts are reported relative to tetramethylsilane.

Amino acid	$^{13}C\beta$ chemical shift (ppm)	
	Measured	Predicted (α-helix/β-sheet)
Ala	18.23	18.30/21.72
Asp	39.72	40.50/42.78
Leu	41.21	41.40/44.02
Met	31.72	31.70/34.34
Ser	62.69	62.81/65.39
Thr	68.68	68.64/70.82

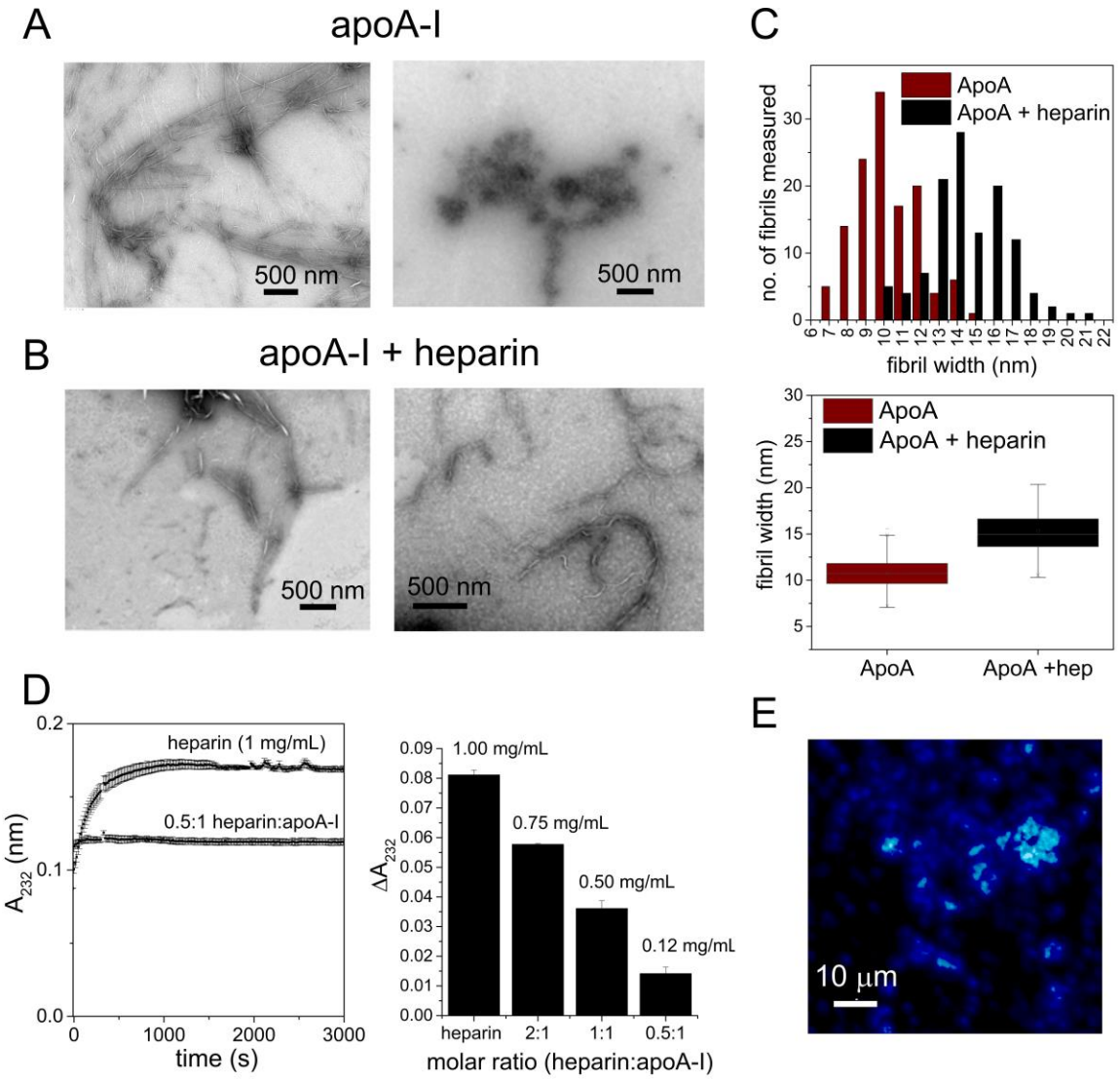

Figure 1. ApoA-I fibril formation in the absence or presence of heparin. (A) Negative stain TEM images of apoA-I aggregates formed at pH 4 in the absence of heparin. (B) TEM images of apoA-I fibrils formed in the presence of 14-15 kDa heparin (2-fold molar excess). (C) Distribution and means of fibril widths measured from TEM images of apoA-I +/- heparin. (D) Determination of heparin association with apoA-I fibrils. Left: time course of uronic acid generation resulting from heparin cleavage by heparinase I. Right: Calculation of heparin remaining in solution following sedimentation with the protein at different molar ratios. ΔA_{232} was measured as the endpoint A_{232} value minus the initial A_{232}. All initial solutions contained 1 mg/ml heparin (~72 μM) before the addition of apoA-I and sedimentation of the aggregates formed. The concentrations shown represent the amount of heparin remaining in solution after removal of the insoluble material. (E) Fluorescence lifetime image (obtained on a Picoquant MicroTime 200 instrument operating at an excitation wavelength of 375 nm) of apoA-I fibrils formed with a 2-fold molar excess of heparin doped with 1 % w/w of a heparin-fluorescein conjugate (ThermoFisher Scientific). Fibrils were washed with aqueous buffer before sedimentation and dispersion onto glass cover slips. The lower image shows the total mean fluorescence lifetime corresponding to a best fitting biexponential curve of time constants 1.5 ns and 4.0 ns.

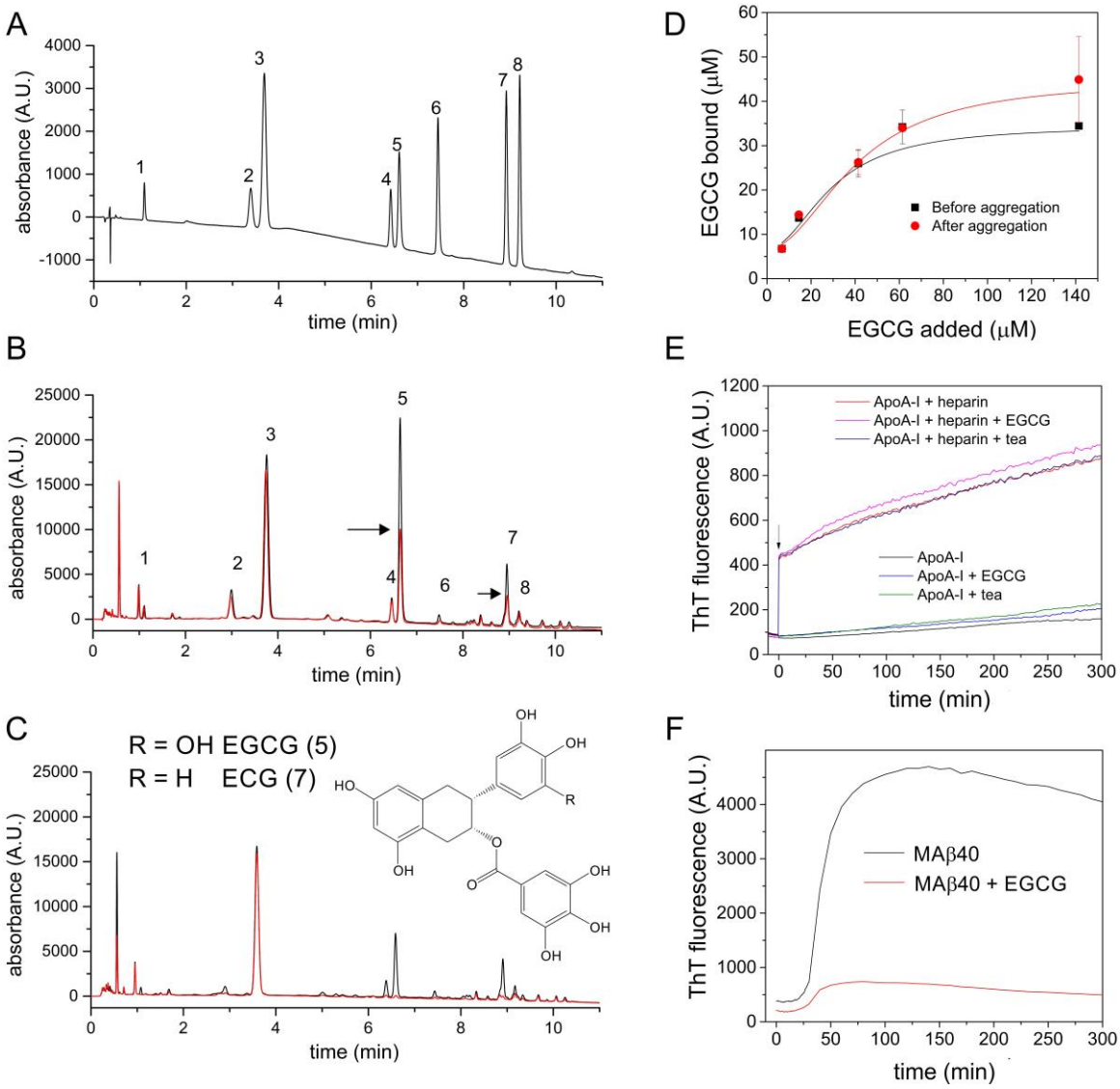

Figure 2. Green tea catechin interactions with apoA-I fibrils. (A) Reverse-phase HPLC analysis of a standard aqueous solution of eight green tea catechins: (1) gallocatechin, (2) caffeine, (3) catechin, (4) epicatechin, (5) epigallocatechin-3-gallate (EGCG), (6) gallocatechin-3-gallate, (7) epicatechin-3-gallate, and (8) catechin-3-gallate. (B) HPLC chromatograms of microwave-extracted green tea solution (black) and the solution after the addition and removal by sedimentation of apoA-I fibrils (red). Arrows highlight the peak height reductions for compounds 5 and 7. (C) Chromatograms of green tea solution (black) and the solution after the addition and removal by sedimentation of MAβ40 fibrils (red). The inset shows the chemical structures of EGCG and ECG. (D) Binding of EGCG to apoA-I. EGCG was added to protein monomer (36 μM) before incubation (black) or to the preformed fibrils (1 mg/mL monomer equivalent; red) as described in Methods. Solid lines represent the best fitting Hill plots, yielding the values of K_d and B_{max} given in the main text. (E) ThT fluorescence for apoA-I incubated in the presence or absence of heparin (2-fold molar excess), and with the addition of EGCG or green tea extract, prior to acidification. The arrow denotes the addition of heparin. (F) ThT fluorescence for Aβ40 fibrils incubated with EGCG. All binding curves and ThT plots represent the mean of three replicate samples.

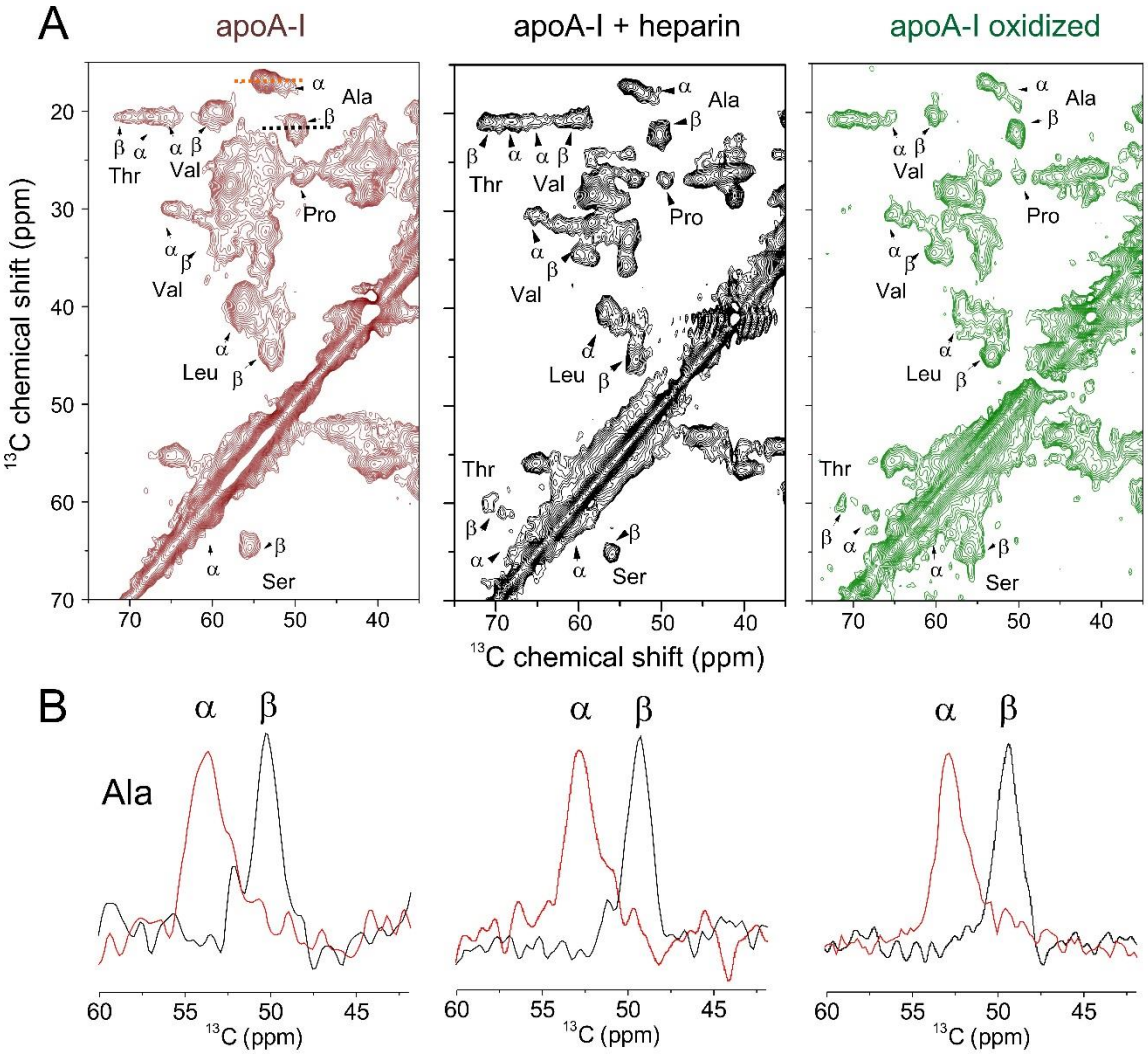

Figure 3. SSNMR suggests a structural similarity of apoA-I fibrils formed under different conditions. (A) 2D ^{13}C-^{13}C solid state NMR spectra (obtained with 20 ms DARR mixing) of uniformly ^{13}C-labelled apoA-I aggregates formed at pH 4 in the absence of heparin (left), in the presence of heparin (centre) or at pH 6 after oxidation (right)). Key assigned cross-peaks are labelled. (B) Horizontal 1D slices through each 2D spectrum at the frequencies of the alanine Cα-Cβ cross peaks, as denoted by the dashed lines in (A). Red peaks occur at the expected chemical shift of alanine within α-helices and black peaks occur at the expected chemical shift of alanine within β-strands.

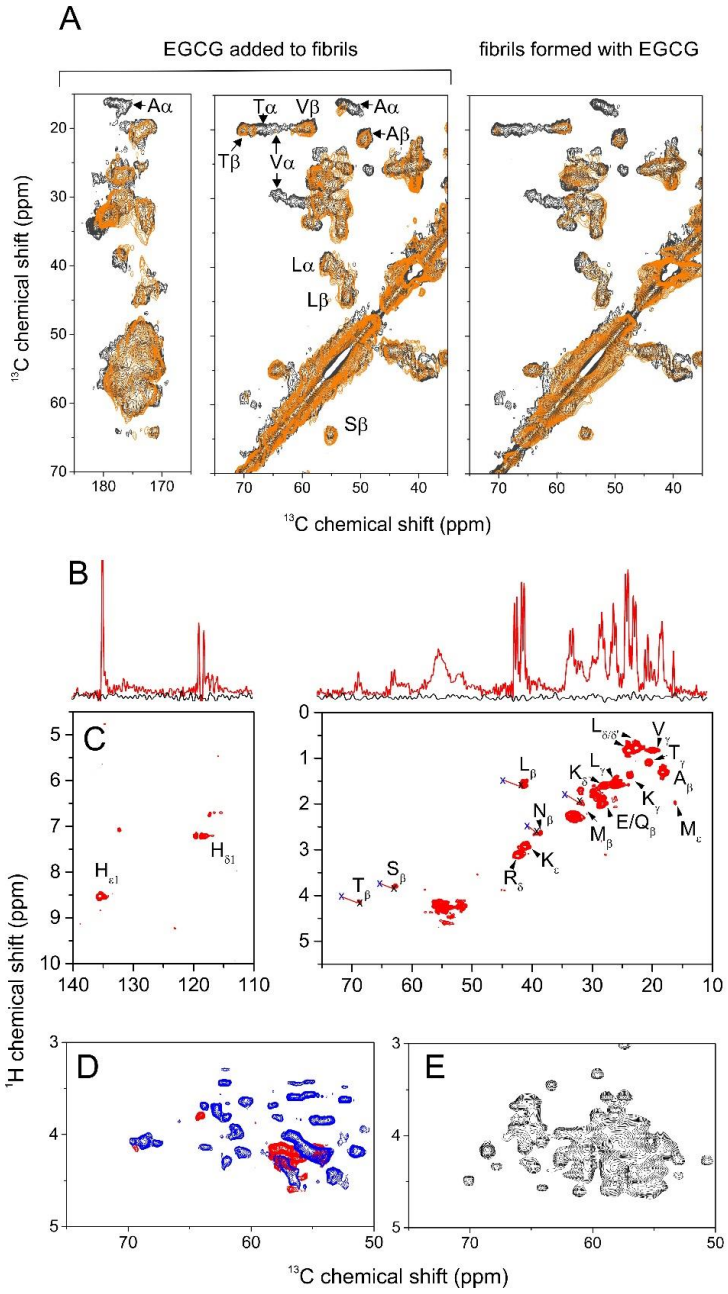

Figure 4. Increased protein mobility after treatment of apoA-I fibrils with EGCG. (A) 2D ^{13}C-^{13}C solid state NMR spectra (obtained with 20 ms DARR mixing) of uniformly ^{13}C-labelled apoA-I aggregates. Spectra are shown for fibrils prepared from 36 μM monomer (black) overlaid with spectra of pre-formed fibrils after isolation and exposure to 36 μM EGCG (left) or overlaid with spectra of fibrils formed from 36 μM monomer in the presence of 36 μM EGCG (right). (B) Regions of 1D ^{13}C INEPT SSNMR spectra of insoluble aggregates (black) and aggregates after exposure to EGCG (red) (C) Corresponding regions of a 2D ^{1}H-^{13}C INEPT spectrum of EGCG-treated fibrils (prepared at pH 4 alone) labelled with assignments for specific amino acids. The blue crosses, linked by red lines to the resonances for T_β, S_β, L_β, N_β and M_β, represent the expected ^{1}H and ^{13}C chemical shifts for those amino acids in β-sheet regions. (D) Spectrum of fibrils formed alone from 36 μM apoA-I monomer and treated with equimolar EGCG (red) or fibrils formed in the presence of 72 μM heparin and treated with 36 μM EGCG (blue). (E) Simulated 2D ^{1}H-^{13}C INEPT spectrum (^{1}Hα-^{13}Cα region only) based on the predicted ^{1}H and ^{13}C chemical shifts of all 243 residues of apoA-I in an α-helical structure.

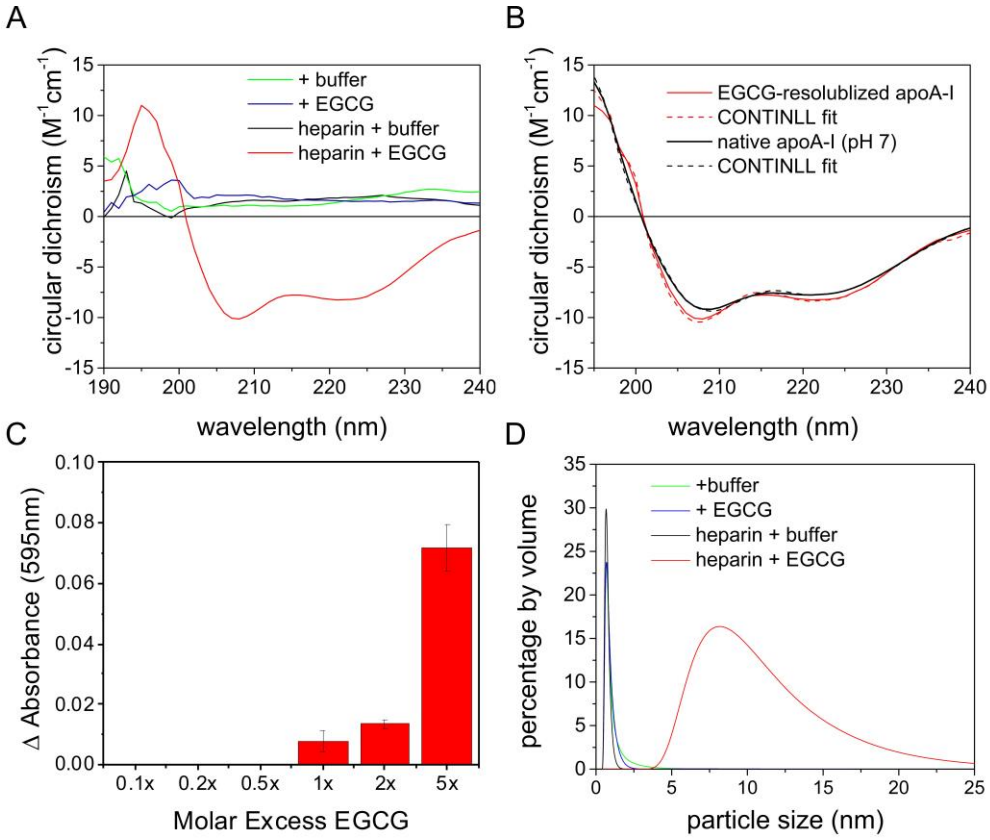

Figure 5. Structure and size of EGCG-remodeled apoA-I fibrils. (A) Far-UV CD spectra of the soluble apoA-I remaining in solution after addition of buffer or EGCG followed by removal of insoluble fibrils. The colour scheme corresponds to fibrils formed in the absence of heparin and incubated with McIlvaine buffer (green) or with EGCG (blue), and fibrils formed in the presence of heparin incubated with buffer only (black) or with EGCG (red). (B) Comparison of the CD spectrum of EGCG-treated fibrils in the presence of heparin with the spectrum of soluble native apoA-I at pH 7 (black). The dotted lines indicate the best fits to the spectra obtained with the CONTINLL algorithm. (C) Analysis using the Bradford reagent indicates that the soluble protein released from fibrils formed in the presence of heparin increases with increasing EGCG concentration up to a 5-fold molar excess over apoA-I. (D) DLS of the supernatant following centrifugation and removal of buffer-treated apoA-I aggregates and apoA-I aggregates treated with EGCG.

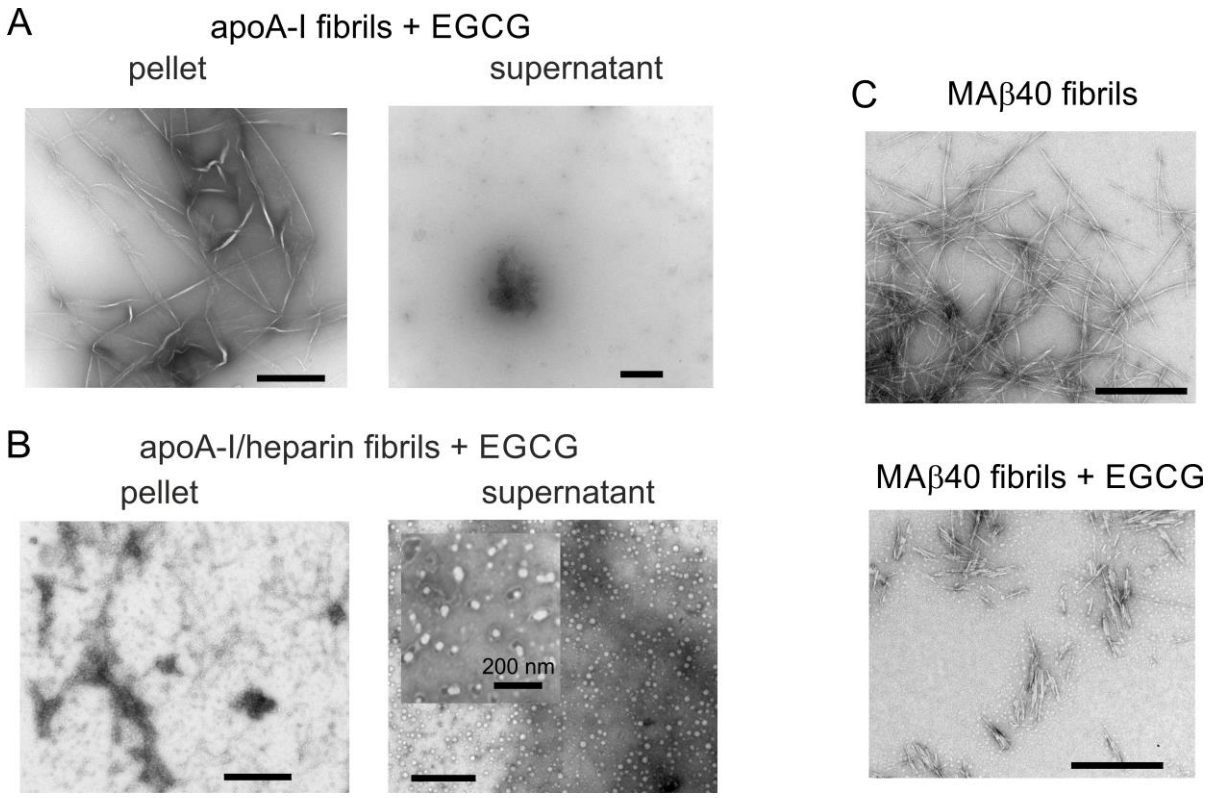

Figure 6. Morphology of EGCG-remodeled apoA-I fibrils (A) Negative stain TEM images of EGCG the insoluble (pellet) and soluble (supernatant) fractions of apoA-I aggregates formed alone or after exposure to EGCG. (B) TEM images of the insoluble and soluble fractions of apoA-I aggregates formed in the presence of heparin before exposure to EGCG. (C) TEM images of MAβ40 fibrils in the absence or presence of EGCG. In each case, fibrils were formed from 36 μM protein monomer alone or in the presence of 72 μM heparin, to which was added buffer or EGCG to a final concentration of 36 μM. All scale bars = 500 nm unless indicated otherwise.

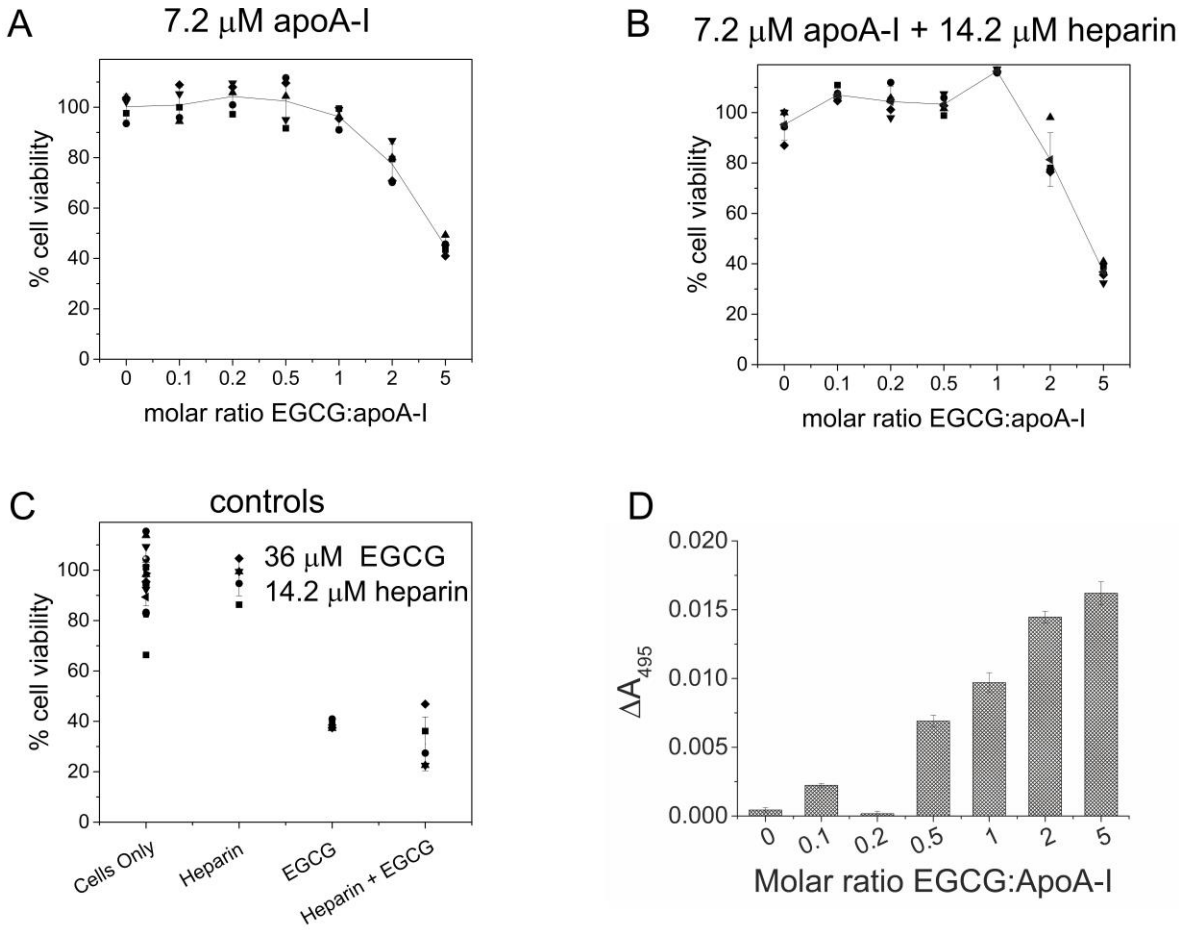

Figure 7. Effect of EGCG-treated apoA-I fibrils on the viability of human umbilical artery endothelial cells. (A) Effect on cell viability of apoA-I fibrils after exposure to different concentrations of EGCG. (B) Effect on cell viability of apoA-1 fibrils formed in the presence of heparin after different concentrations of EGCG. (C) Control measurements of cell viability after the addition of heparin, EGCG or a mixture of both. Means and standard errors are shown for $n = 5$ for each sample group except for the control cells only, for which $n = 15$. (D) Release of heparin from apoA-I fibrils into aqueous solution by the addition of different concentrations of EGCG. Fibrils were formed from 36 μM apoA-I in the presence of 72 μM heparin doped with 1 % w/w fluorescein-heparin conjugate, which was detected by absorbance at 495 nm.

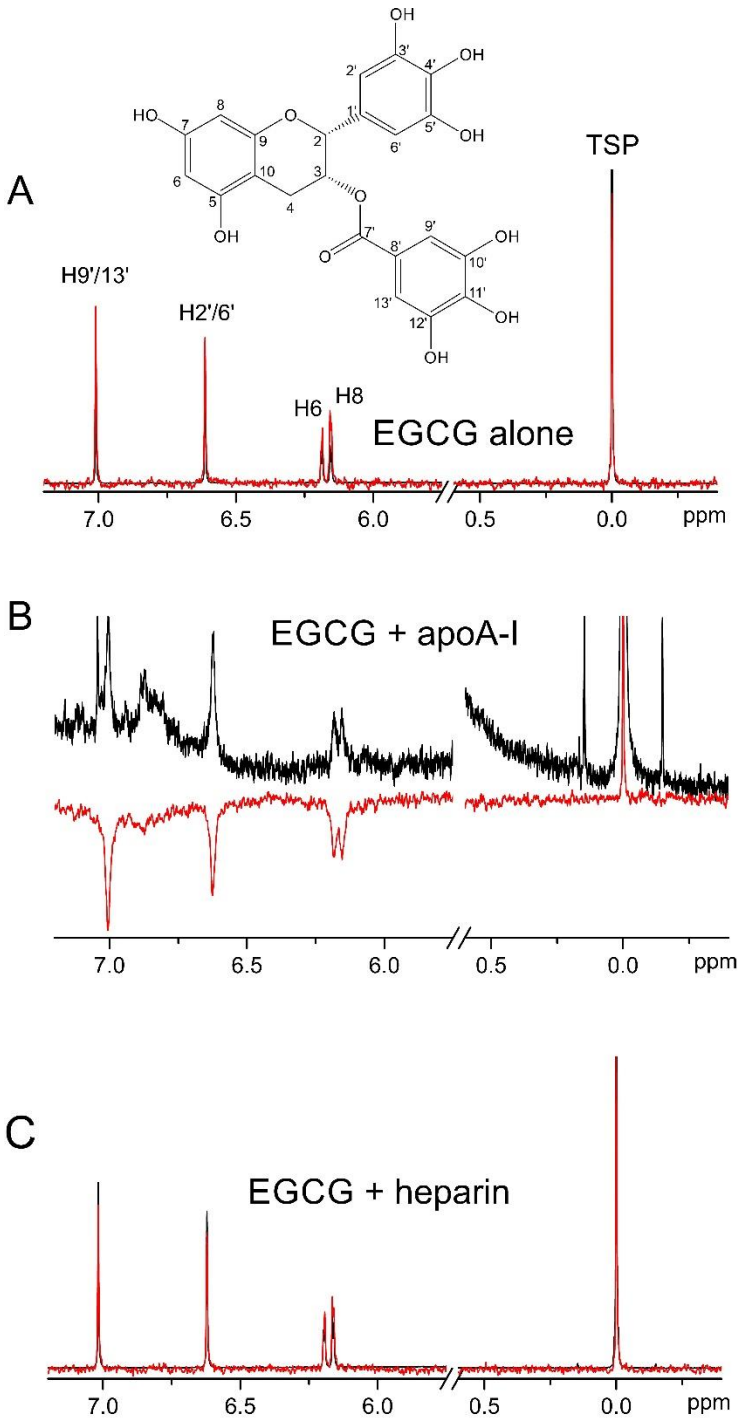

Figure 8. EGCG interactions with apoA-I and heparin. (A) Concentration-dependent effect of EGCG in solubilising heparin from apoA-I fibrils. Fibrils were formed with a 2-fold molar excess of heparin, of which 10 % was the fluorescein conjugate. The absorbance of fluorescein at 496 nm was measured from the supernatant after removal of the insoluble fibrils by centrifugation. (B) Concentration-dependent effect of EGCG in solubilising protein from apoA-I fibrils, measured using the Bradford assay. 1D ^{1}H NMR spectrum (black) and waterLOGSY spectrum (red) of EGCG (720 μM) either (C) alone, (D) in the presence of apoA-I (36 μM), or (E) in the presence of heparin (36 μM).

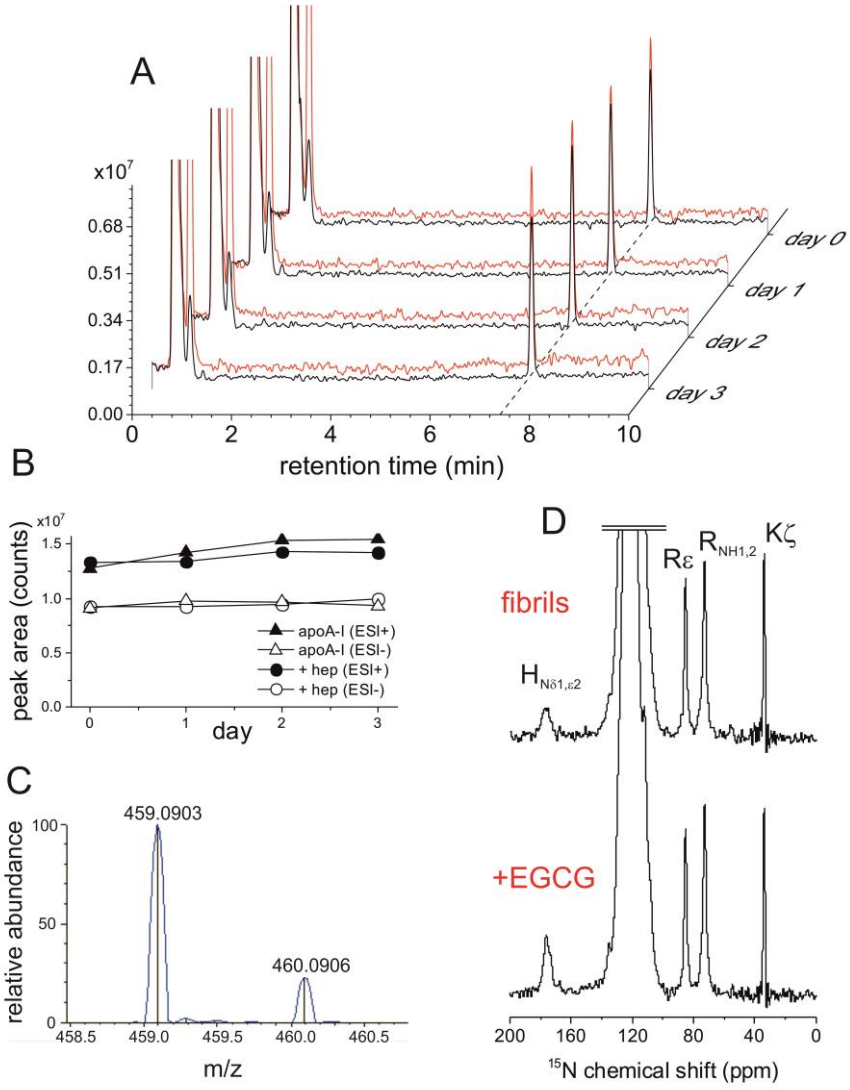

Figure 9. EGCG interacts with apoA-I in the unmodified polyphenol form. (A) LCMS chromatogram of a solution of EGCG incubated with apoA-I for 3 days (after removal of insoluble material), containing positive mode XIC 459.0922 m/z (black), and negative mode XIC 457.0776 m/z (red). (B) Peak areas measured from chromatograms (positive and negative mode XIC) after incubation of EGCG and apoA-I +/- heparin for 0, 1, 2 and 3 days. (C) An example of ESI+ HRMS mass assignment of EGCG at t_R = 7.65 min; 459.0903 m/z measured, 459.0922 m/z predicted for the $C_{22}H_{18}O_{11}$ [M+H]+ ion. (D) Proton-decoupled ^{15}N CP-MAS NMR spectra of uniformly-^{15}N-labeled apoA-I fibrils (prepared at pH 4 in the absence of heparin) before (top) and after (bottom) incubation with EGCG for 24 h.

Epigallocatechin-3-gallate remodels apolipoprotein A-I amyloid fibrils into soluble oligomers in the presence of heparin

David Townsend, Eleri Hughes, Geoffrey Akien, Katie L. Stewart, Sheena E. Radford, David Rochester and David A. Middleton

J. Biol. Chem. published online May 31, 2018
